

Distributed Multiple Fault Detection and Estimation in DC Microgrids with Unknown Power Loads

Jingwei Dong, Mahdiah S. Sadabadi, Per Mattsson, André Teixeira

ABSTRACT. This paper proposes a distributed diagnosis scheme to detect and estimate actuator and power line faults in DC microgrids subject to unknown power loads and stochastic noise. To address actuator faults, we design a fault estimation filter whose parameters are determined through a tractable optimization problem to achieve fault estimation, decoupling from power line faults, and robustness against noise. In contrast, the estimation of power line faults poses greater challenges due to the inherent coupling between fault currents and unknown power loads, which becomes ill-posed when the underlying system is insufficiently excited. To the best of our knowledge, this is the first study to address this critical yet underexplored issue. Our solution introduces a novel differentiate-before-estimate strategy. A set of diagnostic rules based on the temporal characteristics of a constructed residual is developed to distinguish load changes from line faults. Once a power line fault is detected, a regularized least-squares method is activated to estimate the fault currents, for which we further derive an upper bound on the estimation error. Finally, comprehensive simulation results validate the effectiveness of the proposed methods.

1. INTRODUCTION

Microgrids have emerged as pivotal components of modernized power systems, which play a crucial role in enhancing grid resilience and promoting the integration of renewable energy sources and some controllable loads such as electric vehicle chargers [1]. Among them, DC microgrids have gained increasing attention in recent years due to their distinct advantages over AC microgrids, such as higher efficiency, reduced power losses, and greater power transfer capacity [2]. Despite these benefits, the widespread adoption of DC microgrids remains challenging, particularly due to the lack of mature protection schemes to address potential faults in the systems. The low impedance of DC microgrids makes them vulnerable to faults, which can trigger sudden surges in fault currents and cause severe damage to critical devices. If not detected and mitigated promptly, these faults can lead to irreversible damage to the entire system. As a result, the development of effective fault diagnosis schemes has become a crucial research priority to ensure the reliability and resilience of DC microgrids.

Date: August 21, 2025.

The work was supported by the Swedish Research Council under the grant 2021-06316, the Swedish Foundation for Strategic Research, and the Knut and Alice Wallenberg Foundation.

Jingwei Dong, Per Mattsson, and André Teixeira are with the Division of Systems and Control, Uppsala University, Sweden ({jingwei.dong, per.mattsson, andre.teixeira}@it.uu.se). Mahdiah S. Sadabadi is with the Department of Electrical and Electronic Engineering, The University of Manchester, Manchester, U.K. (e-mail: mahdiah.sadabadi@manchester.ac.uk).

1.1. Literature review

The existing results on fault diagnosis of DC microgrids typically focus on fault detection and isolation. The most straightforward way is to set detection thresholds based on characteristics of measured currents and voltages, as presented in [3]. While thresholding-based methods are easy to implement, their diagnosis performance is highly sensitive to the selection of thresholds, which necessitates a thorough understanding of signal properties in both normal and faulty conditions. By exploring additional time-domain information from measured signals, methods based on differential currents [4, 5] and traveling wave analysis [6] can achieve more accurate diagnosis results compared to simple thresholding-based approaches. For instance, the authors in [5] analyzed the first and second derivatives of fault currents to detect DC cable ground faults in the presence of load and operating mode changes. However, such a derivative-based approach is sensitive to noise and may lead to false alarms without a proper selection of thresholds.

In addition to time-domain information, frequency-domain methods, such as fast Fourier transform [7] and wavelet transform [8], are also effective for fault analysis in microgrid systems. Yet, their reliance on case-specific fault frequency characteristics limits their generalization capability. In recent years, the availability of large amounts of historical data has also facilitated the adoption of learning-based approaches in DC microgrid fault diagnosis. A key challenge, however, is the limited amount of data in fault scenarios. We refer interested readers to [9] and [10] for further insights.

Different from signal analysis-based and learning-based approaches, model-based fault diagnosis methods utilize more accurate and comprehensive mathematical models of DC microgrids. This allows for improved robustness against disturbances and lower reliance on data. The basic idea of model-based fault diagnosis methods is to construct residual generators by leveraging model information. When fed measured signals, outputs of the residual generators (called residuals) can indicate the occurrence of faults. Common choices for model-based residual generators include various types of observers, such as Luenberger observers, unknown input observers, and sliding mode observers [11]. In addition, residual generation in the framework of differential-algebraic equations (DAEs) [12] has also gained attention recently.

Let us first briefly review some observer-based fault diagnosis methods developed for DC microgrids. In [13], an unknown input observer was employed to detect arc faults on power lines. To enhance robustness against disturbances while maintaining fault sensitivity, the authors in [14] utilized the mixed $\mathcal{H}_2/\mathcal{H}_\infty$ index in the design of an optimal fault detection observer for DC microgrids. Fault isolation can be achieved by building a bank of observers, each of which is designed to be sensitive to specific faults. For instance, the authors in [15] constructed fault matrices (or signatures) for different types of faults in DC microgrids, and then designed a bank of unknown input observers based on corresponding sensitivity matrices to distinguish fault types. In [16], a bank of unscented Kalman filters was developed to estimate system states under faults, whose outputs were then integrated to locate faulty sensors in DC microgrids. Regarding DAE-based approaches, they offer several advantages over conventional observer-based methods, including: (i) characterizing all possible residual generators for systems described by DAEs, and (ii) deriving residual generators of the lowest possible order [12, 17]. These benefits have also led to the development of anomaly detection methods for microgrid systems within the DAE framework, such as attack detection in [18] and ground fault detection in [19].

Note that the aforementioned methods primarily focus on fault detection and isolation, while research on fault estimation for DC microgrids remains limited. Fault estimation involves determining the shape and size of faults, which has more stringent requirements than fault detection and isolation. The complexity is further exacerbated in DC microgrids with unknown power loads due to the introduction of nonlinearity [20]. To address this issue, the authors in [20] employed a sliding mode observer to estimate actuator and sensor faults in DC microgrids. More recently, an adaptive fault estimation method was developed in [21] to estimate the system states and faults simultaneously. However, both [20] and [21] rely on power line or load current measurements, which require additional sensors that increase system complexity and maintenance costs. The authors in [22] avoided this limitation by proposing a method based on an augmented state observer and an open-loop line current estimator, but the method is confined to addressing sensor attacks.

Based on the above analysis, the problem of multiple fault estimation for DC microgrids remains insufficiently explored, particularly in scenarios where power line currents are unmeasurable and power loads are unknown. Our investigation finds that the coupled effects of fault-induced line currents and unknown power loads pose great challenges in distinguishing between them. This problem is even challenging when the system is not sufficiently excited (e.g., in the case of incipient faults), where the slow variation of signals leads to an ill-posed estimation problem. To the best of our knowledge, this is the first study to address this challenge in the context of DC microgrids.

1.2. Main contributions

This paper proposes a residual-based multiple fault detection and estimation framework for DC microgrids, which takes into account the effects of unknown power loads and stochastic noise. We employ the DAE framework for residual generation, given its aforementioned advantages. Furthermore, considering the scalability issue inherent in centralized diagnosis methods, the proposed diagnosis framework is implemented in a distributed architecture. Specifically, an independent diagnosis component is designed for each distributed generation (DG) unit within the considered DC microgrid, significantly improving its reliability. The contributions of the paper are summarized as follows:

- **Multiple fault estimation framework.** We develop a multiple fault estimation framework for DC microgrids, which accounts for both actuator and power line faults in the presence of measurement noise, unknown power loads, and parametric uncertainties. This framework is built on fault estimation filters developed within the DAE framework, which enables suppression of noise and uncertainties, decoupling of disturbances, and estimation of multiple faults. The filter design with these requirements is then formulated as tractable optimization problems (Proposition 3.1).
- **Differentiation strategy for power line faults and step power load changes.** Building on the practical assumption of piecewise-constant power loads, we propose a novel strategy to distinguish between power line faults and step changes in power loads by exploiting temporal characteristic differences of their effects on residuals (Proposition 4.1). This differentiation process is further formalized into a set of diagnosis rules (Equation (24)), facilitating the subsequent faulty line current estimation.
- **Faulty line current estimation with an explicit error bound.** To address the ill-posed issue in faulty line current estimation, we formulate a regularized least-squares optimization method. An analytical solution is further derived to enable real-time estimation

(Proposition 4.2). Furthermore, we establish a computable bound on the expectation of the estimation error, explicitly characterizing its dependence on load and fault variations (Theorem 4.3).

The structure of the remaining parts of the paper is organized as follows. Section 2 introduces the dynamics of DC microgrids and the problem statement. Section 3 presents the design of the actuator fault estimator, while Section 4 develops the faulty line current estimation method. The proposed methods are validated through simulations in Section 5. Finally, Section 6 concludes the paper. For readability, some technical proofs are relegated to Appendix.

Notation. The sets \mathbb{N} , \mathbb{R} (\mathbb{R}_+), and \mathbb{R}^n denote non-negative integers, (positive) reals, and the space of n dimensional real-valued vectors, respectively. The space of $n \times n$ dimensional symmetric matrices is denoted by \mathbb{S}^n . The identity matrix of the size n is denoted by \mathbf{I}_n . For a random variable χ , the probability law and the expectation are denoted by $\mathbf{Pr}[\chi]$, and $\mathbf{E}[\chi]$, respectively. For a vector $x = [x_1, \dots, x_n]^\top \in \mathbb{R}^n$, the 2-norm of x is $\|x\|_2 = \sqrt{\sum_{i=1}^n x_i^2}$. For a matrix $A \in \mathbb{R}^{m \times n}$, its transpose and pseudo-inverse are denoted by A^\top and A^\dagger , respectively. The 2-norm of A is denoted by $\|A\|_2$, which represents the largest singular value of A , i.e. $\bar{\sigma}(A)$. If A is a square matrix, its smallest and largest eigenvalues are denoted by $\underline{\lambda}_A$ and $\bar{\lambda}_A$, respectively. We use $Q \succ 0$ ($Q \prec 0$) to denote a positive (negative) definite matrix Q . For a discrete-time signal $r(k)$, the stacked data vector of the length T is denoted by $\mathbf{r}_T(k) = [r^\top(k-T+1) \ \dots \ r^\top(k)]^\top$.

2. MODEL DESCRIPTION AND PROBLEM STATEMENT

We recall the dynamic model of a Kron-reduced DC microgrid composed of n power-electronics-interfaced DG units, which are connected by m power lines. The index sets of DG units and lines are denoted as \mathbb{N}_G and \mathbb{N}_L , respectively. Fig. 1 illustrates the architecture of a DC microgrid with 3 DG units and 2 power lines. In the subsequent parts of this section, we will elaborate on the dynamics of each individual component within the microgrid.

2.1. DG Dynamics

Each DG unit includes a DC input voltage source $V_{dc,i}$, a DC-DC buck converter, and a resistive-inductive-capacitive filter with the parameters $(R_{t,i}, L_{t,i}, C_{t,i})$. This configuration is illustrated in the dashed box of Fig. 1, which depicts the circuit diagram of DG unit 1 connected to DG unit 2 via power line 1. Using the circuit theory, for each $i \in \mathbb{N}_G$, the dynamics of DG unit i are presented by [23]:

$$\begin{cases} C_{t,i} \dot{V}_i(t) = I_{t,i}(t) - P_i(t)/V_i(t) - \sum_{k=1}^m \mathbb{B}_{ik} I_k(t), \\ L_{t,i} \dot{I}_{t,i}(t) = -V_i(t) - R_{t,i} I_{t,i}(t) + u_i(t) + f_{a,i}(t), \end{cases} \quad (1)$$

where $V_i(t) \in \mathbb{R}$ and $I_{t,i}(t) \in \mathbb{R}$ are the voltage at the Point of Common Coupling (PCC) i and the filter current, respectively. The unknown power demand is denoted by $P_i(t) \in \mathbb{R}_+$. The control signal $u_i(t) = \varphi_i(t)V_{dc,i}$, where $\varphi_i(t)$ is the duty cycle of the buck converter. The current of power line k is represented by $I_k(t) \in \mathbb{R}$ where $k \in \mathbb{N}_L$. The microgrid topology is encoded in the incidence matrix element \mathbb{B}_{ik} , which indicates the connection between power line k and DG unit i . In particular, $\mathbb{B}_{ik} = 1$ if DG i is the positive end of line k , $\mathbb{B}_{ik} = -1$ if DG i is the negative end of line k , and $\mathbb{B}_{ik} = 0$ otherwise. Therefore, the term $\sum_{k=1}^m \mathbb{B}_{ik} I_k(t)$ is the total current injected into DG i from its neighbors and represents the physical couplings of DG i with neighboring DG units. The additive actuator fault in DG unit i is denoted by $f_{a,i}(t) \in \mathbb{R}$.

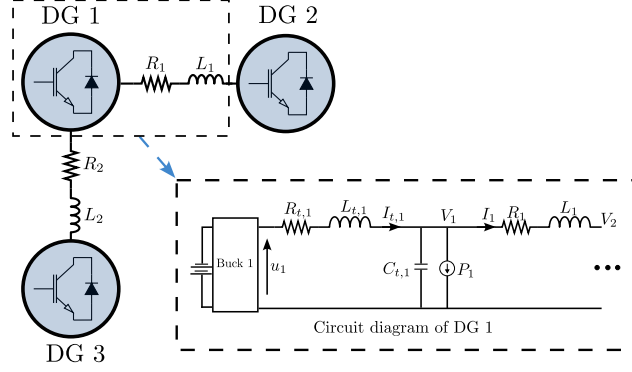


FIGURE 1. Structure of a DC microgrid.

2.2. Power Line Dynamics

The DG units are coupled to their neighbors through resistive-inductive power lines. For $k \in \mathbb{N}_L$, the dynamics of the line current $I_k(t)$ are governed by

$$\dot{I}_k(t) = -\frac{R_k}{L_k}I_k(t) + \frac{1}{L_k} \sum_{j=1}^n \mathbb{B}_{jk}V_j(t) + f_{L,k}(t), \quad (2)$$

where R_k is the line resistance and L_k is the line inductance. The fault on line k is denoted by $f_{L,k}(t) \in \mathbb{R}$.

Assumption 2.1 (Unmeasurable line currents and uncertain parameters). *The line currents are unmeasurable, and the parameters R_k and L_k can be identified with uncertainty in the fault-free condition.*

According to the superposition principle, the line current $I_k(t)$ consists of a fault-free component $I_{k,h}(t)$, a fault component $I_{k,f}(t)$, and a noise term ϵ_k induced by uncertainty, i.e., $I_k(t) = I_{k,h}(t) + I_{k,f}(t) + \epsilon_k(t)$.

Remark 2.2 (Applicability beyond additive faults). *Although the power line faults considered in (2) are additive, other types of faults, such as short-circuit faults that change the dynamics of I_k , can be represented within this framework as well. A pole-to-ground short-circuit fault will be demonstrated in Section 6 to illustrate this applicability.*

2.3. Stabilizing Voltage Controller

For the purpose of voltage control, each DG unit is equipped with a local voltage controller (VC), which is given by:

$$\begin{cases} u_i(t) = k_{1,i}V_i(t) + k_{2,i}I_{t,i}(t) + k_{3,i}v_i(t), \\ \dot{v}_i(t) = V_i^* - V_i(t), \end{cases} \quad (3)$$

where V_i^* is a reference voltage provided by a higher-level controller, $K_i = [k_{1,i} \ k_{2,i} \ k_{3,i}]$ is the voltage control gain vector. Design methods for K_i can be found in [24] or [25].

2.4. Closed-loop Dynamics

With (1)-(3), the closed-loop dynamics of DG i for $i \in \mathbb{N}_G$ can be written as:

$$\begin{cases} \dot{x}_i(t) = A_i x_i(t) + B_i V_i^* + D_i d_i(t) + E_i f_{a,i}(t) + \delta_i(t), \\ y_i(t) = C_i x_i(t) + \zeta_i(t), \end{cases} \quad (4)$$

where $x_i = [V_i \ I_{t,i} \ v_i]^T$, δ_i , y_i , and ζ_i denote the state, process noise, output, and measurement noise, respectively. The signal d_i consists of the power load P_i and currents injected from all power lines connected to DG unit i , i.e.,

$$\begin{aligned} d_i(t) &= P_i(t)/V_i(t) + \sum_{k=1}^m \mathbb{B}_{ik} I_k(t) \\ &= P_i(t)/V_i(t) + \sum_{k=1}^m (\mathbb{B}_{ik} I_{k,h}(t) + \epsilon_k(t)) + f_{I,i}(t), \end{aligned}$$

where $f_{I,i}(t) = \sum_{k=1}^m \mathbb{B}_{ik} I_{k,f}(t)$ denote the aggregated faulty line current affecting DG unit i . The system matrices in (4) are as follows:

$$A_i = \begin{bmatrix} 0 & \frac{1}{C_{t,i}} & 0 \\ \frac{k_{1,i}-1}{L_{t,i}} & \frac{k_{2,i}-R_{t,i}}{L_{t,i}} & \frac{k_{3,i}}{L_{t,i}} \\ -1 & 0 & 0 \end{bmatrix}, \quad B_i = \begin{bmatrix} 0 \\ 0 \\ 1 \end{bmatrix}, \quad D_i = \begin{bmatrix} -\frac{1}{C_{t,i}} \\ 0 \\ 0 \end{bmatrix}, \quad E_i = \begin{bmatrix} 0 \\ \frac{1}{L_{t,i}} \\ 0 \end{bmatrix}, \quad C_i = \mathbf{I}_3.$$

Since the voltage V_i and the filter current $I_{t,i}$ are measurable [26], and v_i is the controller variable, we have full state measurement here, i.e., $C_i = \mathbf{I}_3$. Let us further introduce the following assumption on noise.

Assumption 2.3 (Stochastic noise). *The noise terms δ_i , ϵ_k , and ζ_i for $i \in \mathbb{N}_G$ and $k \in \mathbb{N}_L$ are mutually uncorrelated zero-mean stochastic processes of unknown distributions. Their covariance matrices denoted by Σ_{δ_i} , Σ_{ϵ_k} and Σ_{ζ_i} are known.*

The covariance matrices Σ_{δ_i} , Σ_{ϵ_k} and Σ_{ζ_i} can be computed from available information about the local models, sensors, and possibly on historical data through Monte Carlo-based approaches [27], and a discussion of their computational approach can be found in [28]. In addition, we account for unmodeled system uncertainties within the stochastic process noise, as commonly adopted in literature [29, Section 3.4].

2.5. Problem Statement.

This work aims to develop a distributed method to detect and estimate both the actuator fault $f_{a,i}$ and the aggregated faulty line current $f_{I,i}$ in DG unit i , while accounting for the unknown power load P_i and the noise terms δ_i , ϵ_k , and ζ_i . Estimating $f_{a,i}$ is relatively straightforward, as it is the only unknown signal in the dynamics of the measurable current $I_{t,i}$ in (1). However, it is challenging to even detect $f_{I,i}$ because the line current I_k is unavailable and $f_{I,i}$ is coupled with P_i in d_i , as described in (4). It is worth noting that $f_{I,i}$ and P_i are indistinguishable in the following two cases:

- (1) **Arbitrarily varying P_i and $f_{I,i}$.** If $P_i(t)$ and $f_{I,i}(t)$ can take any values, different combinations of $P_i(t)$ and $f_{I,i}(t)$ can yield identical total values and result in an indistinguishable scenario. For instance, consider two different pairs, $(P_i(t), f_{I,i}(t))$ and $(P'_i(t), f'_{I,i}(t))$. It

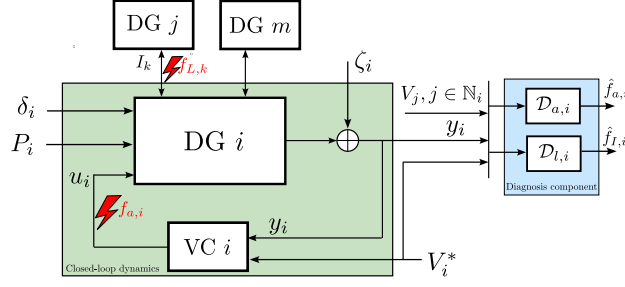


FIGURE 2. Structure of DG i with the diagnosis component: block $\mathcal{D}_{a,i}$ for the actuator fault $f_{a,i}$ and block $\mathcal{D}_{l,i}$ for the aggregate faulty line current $f_{l,i}$, where \mathbb{N}_i denote the set of neighboring units of DG i .

holds that

$$\frac{P_i(t)}{V_i(t)} + f_{l,i}(t) = \frac{P'_i(t)}{V_i(t)} + f'_{l,i}(t),$$

if $P'_i(t) = (P_i(t)/V_i(t) + f_{l,i}(t) - f'_{l,i}(t))V_i(t)$.

- (2) **Constant V_i .** If $V_i(t)$ is constant, separation of $f_{l,i}$ and P_i is theoretically impossible because the signal V_i does not provide sufficient variation to distinguish their contributions in the aggregated signal $P_i/V_i + f_{l,i}$. This is close to the well-known persistence of excitation phenomena for LTI systems, as discussed in [30, Theorem 3.5]. It is also reflected in the rank condition following (25) in Subsection 4.4.

Fortunately, in practical DC microgrids, power loads do not vary arbitrarily but typically follow specific patterns. Various types of loads, such as data centers, electric vehicle charging stations, motor drives, and inverter-based AC loads, can be approximated as constant power loads [1, 31]. Based on this observation, the following assumption about P_i is made throughout the paper to exclude the first scenario where P_i and $f_{l,i}$ become indistinguishable. We emphasize that no assumption is imposed on the fault signals.

Assumption 2.4 (Piece-wise constant power load). *The power load $P_i(t)$ is a piece-wise constant signal, with each value persisting for a sufficiently large duration.*

In the second indistinguishable case, although both faults and load changes can cause variations in V_i , these effects are rapidly attenuated by feedback control, particularly in scenarios involving incipient faults or step load changes. As a result, V_i typically exhibits slow variations or converges to a constant value, rendering the estimation problem of $f_{l,i}$ from $P_i/V_i + f_{l,i}$ ill-posed.

We are now in the position to formally present the problems studied in this paper. To address actuator and power line faults in DC microgrids, we design a diagnosis component for each DG unit, as illustrated in Fig. 2. The diagnosis component consists of two blocks: $\mathcal{D}_{a,i}$ used to estimate the actuator fault $f_{a,i}$ and $\mathcal{D}_{l,i}$ used to estimate the aggregate faulty line current $f_{l,i}$. The inputs to the diagnosis component are known signals, including V_i^* , y_i , and V_j received from neighboring DG units. The outputs are the estimates of $f_{a,i}$ and $f_{l,i}$, denoted by $\hat{f}_{a,i}$ and $\hat{f}_{l,i}$, respectively.

Our objective is to design $\mathcal{D}_{a,i}$ and $\mathcal{D}_{l,i}$ to achieve real-time estimation of $f_{a,i}$ and $f_{l,i}$ in DG unit i . Specifically, the design requirements for $\mathcal{D}_{a,i}$ are as follows:

- (1) The effects of influencing factors (e.g., $f_{l,i}$ and P_i) on the estimated value $\hat{f}_{a,i}$ should be decoupled;

- (2) The estimation result should be robust to noise signals δ_i , ϵ_k , and ζ_i ;
- (3) Given the stochastic nature of noise, the steady-state estimation error of $f_{a,i}$ should converge to zero in expectation, i.e., $\lim_{t \rightarrow \infty} |\mathbf{E}[\hat{f}_{a,i}(t) - f_{a,i}(t)]| \rightarrow 0$.

The design requirements for $\mathcal{D}_{l,i}$ include:

- (1) The effect of $f_{a,i}$ is decoupled from the estimated value $\hat{f}_{l,i}$;
- (2) The estimation result should be robust to noise signals δ_i , ϵ_k , and ζ_i ;
- (3) Given the possibly ill-posed issue due to the load term P_i/V_i , rather than enforcing convergence of the estimation error to zero, we instead require the estimation error for $f_{l,i}$ to be bounded in expectation, as follows:

$$\left| \mathbf{E} \left[\hat{f}_{l,i}(t) - \bar{f}_{l,i}(t) \right] \right| \leq \mathcal{C}(y_i, V_i^*, V_j, P_i, f_{l,i}),$$

where $\bar{f}_{l,i}(t)$ represents the average value of $f_{l,i}(t)$ over a period, $\mathcal{C}(\cdot)$ is a time-varying bound dependent on the system and power line dynamics (2)-(4), input signals to $\mathcal{D}_{l,i}$, and properties of unknown signals P_i and $f_{l,i}$.

3. ESTIMATION OF ACTUATOR FAULTS

In this section, we provide the design method for $\mathcal{D}_{a,i}$. A fault estimation filter is developed as the core solution. To facilitate the filter design, the state-space model (4) is reformulated into the DAE form:

$$H_i(p)X_i + \mathcal{B}_i Y_i + \mathcal{E}_i f_{a,i} + \omega_i = 0, \quad (5)$$

where p is the derivative operator, i.e., $\dot{x}(t) = px(t)$, the augmented variables $X_i = [x_i^\top \ d_i]^\top$, $\omega_i = [\delta_i^\top \ \zeta_i^\top]^\top$, and $Y_i = [y_i^\top \ V_i^*]^\top$. The polynomial matrix $H_i(p)$ is defined as

$$H_i(p) = pH_{i,1} + H_{i,0} = \begin{bmatrix} -p\mathbf{I}_3 + A_i & D_i \\ C_i & \mathbf{0}_{3 \times 1} \end{bmatrix},$$

where

$$H_{i,1} = \begin{bmatrix} -\mathbf{I}_3 & \mathbf{0}_{3 \times 1} \\ \mathbf{0}_{3 \times 3} & \mathbf{0}_{3 \times 1} \end{bmatrix}, \quad H_{i,0} = \begin{bmatrix} A_i & D_i \\ C_i & \mathbf{0}_{3 \times 1} \end{bmatrix}.$$

The matrices \mathcal{B}_i and \mathcal{E}_i are given by

$$\mathcal{B}_i = \begin{bmatrix} \mathbf{0}_{3 \times 3} & B_i \\ -\mathbf{I}_3 & \mathbf{0}_{3 \times 1} \end{bmatrix}, \quad \mathcal{E}_i = \begin{bmatrix} E_i \\ \mathbf{0}_{3 \times 1} \end{bmatrix}.$$

Then, we consider the estimation filter for actuator faults in the following form:

$$\hat{f}_{a,i} = -\frac{N_i(p)\mathcal{B}_i}{a(p)}Y_i, \quad (6)$$

where the polynomial row vector $N_i(p) = \sum_{j=0}^{d_N} p^j N_{i,j}$, $N_{i,j} \in \mathbb{R}^{1 \times 6}$ and d_N is the degree of $N_i(p)$. The denominator $a(p)$ is a polynomial defined as $a(p) = p^{d_a} + \sum_{j=0}^{d_a-1} p^j a_j$, where d_a denotes the degree of $a(p)$ and the coefficients $a_j \in \mathbb{R}$. For simplicity of filter design, $a(p)$ is given with all roots lying in the left-half plane and is identical for all $\mathcal{D}_{a,i}$. Its degree is set as $d_a = d_N + 1$ to ensure that the filter is strictly proper.

By multiplying the left-hand side of (5) by $N_i(p)/a(p)$, $\hat{f}_{a,i}$ can be expressed as

$$\hat{f}_{a,i} = \frac{N_i(p)H_i(p)}{a(p)}X_i + \frac{N_i(p)\mathcal{E}_i}{a(p)}f_{a,i} + \frac{N_i(p)}{a(p)}\omega_i. \quad (7)$$

Note that (6) can be used to generate $\hat{f}_{a,i}$, as all elements are measurable or known, while (7) explicitly characterizes the mapping relations from X_i , $f_{a,i}$, and ω_i to $\hat{f}_{a,i}$, thus providing the foundation for designing the filter parameters.

Recall the first design requirement for $\mathcal{D}_{a,i}$, which stipulates that P_i and $f_{I,i}$ have no influence on $\hat{f}_{a,i}$. To achieve this, we introduce the following condition

$$N_i(p)H_i(p) = 0, \quad (8a)$$

which ensures that the signal X_i implicitly containing P_i and $f_{I,i}$ is completely decoupled from $\hat{f}_{a,i}$. To address the second design requirement regarding robustness against stochastic noise, we employ the \mathcal{H}_2 norm approach. For a linear system driven by white noise with zero mean, the \mathcal{H}_2 norm of its transfer function represents the asymptotic variance of the output [32]. Therefore, the second design requirement can be realized by constraining the \mathcal{H}_2 norm of $N_i(p)/a(p)$ as follows

$$\left\| \frac{N_i(p)}{a(p)} \right\|_{\mathcal{H}_2}^2 \leq \gamma_i, \quad (8b)$$

where $\gamma_i \in \mathbb{R}_+$ is an upper bound. To guarantee convergence of the fault estimate, i.e., $\hat{f}_{a,i} \rightarrow f_{a,i}$ in the steady state, we impose a unity steady state gain constraint on the transfer function $N_i(p)\mathcal{E}_i/a(p)$, which is

$$\left. \frac{N_i(p)\mathcal{E}_i}{a(p)} \right|_{p=0} = 1. \quad (8c)$$

Based on (7), the design requirements for $\mathcal{D}_{a,i}$ have been translated into constraints (8a)-(8c) on the mapping relations. In the following proposition, we further formulate a tractable optimization problem for solving the parameters of $N_i(p)$ based on (8a)-(8c). Before proceeding, the observable canonical form of $N_i(p)/a(p)$, denoted by $\{A_r, B_{r,i}, C_r\}$, is provided to facilitate computation of the \mathcal{H}_2 norm. Here, A_r is given by the coefficients of $a(p)$, which we keep the same for all i , while $B_{r,i}$ is different for different i . Specifically, the matrices are given by

$$A_r = \begin{bmatrix} 0 & \dots & 0 & -a_0 \\ 1 & \dots & 0 & -a_1 \\ \vdots & \ddots & \vdots & \vdots \\ 0 & \dots & 1 & -a_{d_N} \end{bmatrix}, \quad B_{r,i} = \begin{bmatrix} N_{i,0} \\ N_{i,1} \\ \vdots \\ N_{i,d_N} \end{bmatrix}, \quad C_r = [0 \quad \dots \quad 0 \quad 1]. \quad (9)$$

The design approach of the actuator fault estimation filter is then presented in the following proposition.

Proposition 3.1 (Actuator fault estimation). *Consider the closed-loop dynamics of DG unit i (for $i \in \mathbb{N}_G$) in (4) subject to the actuator fault $f_{a,i}$. The design conditions (8a)-(8c) for the estimation filter structured in (6) can be equivalently formulated into the following linear programming problem:*

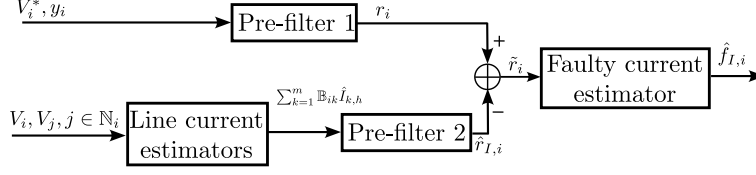
$$\min \gamma_i$$

$$\text{s.t. } N_{i,j} \in \mathbb{R}^{1 \times 6}, j \in \{0, 1, \dots, d_N\}, Q_i \in \mathbb{S}^{d_N+1}, \gamma_i \in \mathbb{R}_+,$$

$$[N_{i,0} \quad N_{i,1} \quad \dots \quad N_{i,d_N}] \bar{H}_i = 0, \quad (10a)$$

$$N_{i,0}\mathcal{E}_i = a(0), \quad (10b)$$

$$\begin{bmatrix} A_r Q_i + Q_i A_r^\top & B_{r,i} \\ B_{r,i}^\top & -\mathbf{I}_6 \end{bmatrix} \prec 0, \quad \begin{bmatrix} \gamma_i & C_r Q_i \\ Q_i C_r^\top & Q_i \end{bmatrix} \succ 0, \quad (10c)$$

FIGURE 3. Structure of the diagnosis block $\mathcal{D}_{l,i}$.

where \bar{H}_i is given by

$$\bar{H}_i = \begin{bmatrix} H_{i,0} & H_{i,1} & \mathbf{0} & \dots & \mathbf{0} \\ \mathbf{0} & H_{i,0} & H_{i,1} & \dots & \mathbf{0} \\ \vdots & \ddots & \ddots & \ddots & \vdots \\ \mathbf{0} & \dots & \mathbf{0} & H_{i,0} & H_{i,1} \end{bmatrix}.$$

Proof. The proof is similar to that of Theorem 3.1 from [33] and thus is omitted here. \square

The feasibility of (10) depends on the rank properties of \bar{H}_i and \mathcal{E}_i . Specifically, the condition for (10a) to have non-trivial solutions is that \bar{H}_i does not have full row rank. This can be satisfied by selecting the numerator degree of the filter d_N such that $6(d_N + 1) > \text{rank}(\bar{H}_i)$, where $6(d_N + 1)$ is the row number of \bar{H}_i . Meanwhile, since all roots of $a(p)$ are in the left-half plane, $a(0) \neq 0$ is guaranteed. Consequently, (10b) requires that \mathcal{E}_i lies outside the column range space of \bar{H}_i , i.e., $\text{rank}([\bar{H}_i \ \mathcal{E}_i]) > \text{rank}(\bar{H}_i)$. Otherwise, a feasible solution to $N_{i,0}\bar{H}_i = 0$ leads to $N_{i,0}\mathcal{E}_i = 0$ as well, and (10b) is not satisfied.

4. ESTIMATION OF AGGREGATE FAULTY LINE CURRENT

In this section, we present the design method for the diagnosis block $\mathcal{D}_{l,i}$, which estimates the aggregate faulty line current $f_{l,i}$ induced by faults on power lines connected to DG unit i . As shown in Fig. 3, $\mathcal{D}_{l,i}$ consists of four sub-blocks:

- (1) Pre-filter 1 that decouples the actuator fault $f_{a,i}$ and generates output $r_i \in \mathbb{R}$.
- (2) A set of line current estimators to estimate the fault-free part of the total line currents $\sum_{k=1}^m \mathbb{B}_{ik} I_k$ injected into DG unit i , which produces $\sum_{k=1}^m \mathbb{B}_{ik} \hat{I}_{k,h}$.
- (3) Pre-filter 2 that produces processed output $\hat{r}_{l,i} \in \mathbb{R}$.
- (4) A faulty current estimator that generates the estimated value $\hat{f}_{l,i}$ using the difference between r_i and $\hat{r}_{l,i}$.

In what follows, we provide a detailed elaboration on the functions and design methods for these sub-blocks.

4.1. Design of Pre-filter 1

The design of Pre-filter 1 is similar to that of the actuator fault estimation filter (6). We first reformulate the closed-loop dynamics (4) into the DAE form:

$$\mathcal{H}_i(p)\mathcal{X}_i + \mathcal{B}_i Y_i + \mathcal{G}_i d_i + \omega_i = 0, \quad (11)$$

where $\mathcal{X}_i = [x_i^\top \ f_{a,i}^\top]^\top$. The polynomial matrix $\mathcal{H}_i(p)$ is obtained by replacing D_i with E_i in $H_i(p)$ from previous DAE (5). The matrix \mathcal{G}_i is defined as $\mathcal{G}_i = [D_i^\top \ \mathbf{0}_{3 \times 1}^\top]^\top$. The rest terms remain

consistent with (5). The structure of Pre-filter 1 mirrors (6) and is given by

$$r_i = -\frac{\mathcal{N}_i(p)\mathcal{B}_i}{a(p)}Y_i, \quad (12)$$

where $\mathcal{N}_i(p) = \sum_{j=0}^{d_{\mathcal{N}}} p^j \mathcal{N}_{i,j}$ with design parameters $\mathcal{N}_{i,j} \in \mathbb{R}^{1 \times 6}$ and degree $d_{\mathcal{N}}$. The denominator $a(p)$ is the same as that in (6). From (11) and (12), r_i also equals to

$$r_i = \frac{\mathcal{N}_i(p)\mathcal{H}_i(p)}{a(p)}\mathcal{X}_i + \frac{\mathcal{N}_i(p)\mathcal{G}_i}{a(p)}d_i + \frac{\mathcal{N}_i(p)}{a(p)}\omega_i.$$

Recall the first two design requirements for $\mathcal{D}_{l,i}$. To decouple $f_{a,i}$ and suppress the effects of ω_i , similar conditions as (8a)-(8c) are employed here to design $\mathcal{N}_i(p)$, which are

$$\mathcal{N}_i(p)\mathcal{H}_i(p) = 0, \quad \left. \frac{\mathcal{N}_i(p)\mathcal{G}_i}{a(p)} \right|_{p=0} = 1, \quad \left\| \frac{\mathcal{N}_i(p)}{a(p)} \right\|_{\mathcal{H}_2}^2 \leq \tilde{\gamma}_i,$$

where $\tilde{\gamma}_i \in \mathbb{R}_+$ is an upper bound. Subsequently, the coefficients of $\mathcal{N}_i(p)$ can be solved using the method in Proposition 3.1. Since \mathcal{X}_i has been decoupled by the derived Pre-filter 1, r_i becomes

$$r_i = \frac{\mathcal{N}_i(p)\mathcal{G}_i}{a(p)} \left(\sum_{k=1}^m \mathbb{B}_{ik}I_k + \frac{P_i}{V_i} \right) + \frac{\mathcal{N}_i(p)}{a(p)}\omega_i, \quad (13)$$

with $d_i(t) = P_i(t)/V_i(t) + \sum_{k=1}^m \mathbb{B}_{ik}I_k(t)$ defined after (4).

4.2. Design of Line Current Estimators

Based on the power line dynamics given in (2), an open-loop estimator is employed here to estimate the fault-free component of I_k for each $k \in \mathbb{N}_L$, as follows:

$$\dot{\hat{I}}_{k,h}(t) = -\frac{R_k}{L_k}\hat{I}_{k,h}(t) + \frac{1}{L_k} \sum_{j=1}^n \mathbb{B}_{jk}V_j(t). \quad (14)$$

In the absence of faults and noise, the dynamics of the estimation error $\tilde{I}_k = I_k - \hat{I}_{k,h}$ can be described by: $\dot{\tilde{I}}_k(t) = -R_k/L_k \tilde{I}_k(t)$. Since \tilde{I}_k converges to zero asymptotically, we can replace $I_{k,h}$ with $\hat{I}_{k,h}$ in the subsequent analysis. When taking faults and noise into account, \tilde{I}_k becomes:

$$\tilde{I}_k = I_k - \hat{I}_{k,h} \approx I_k - I_{k,h} = I_{k,f} + \epsilon_k. \quad (15)$$

Given the asymptotic convergence speed, we suppose $\tilde{I}_k = I_{k,f} + \epsilon_k$ for the remainder of the paper.

4.3. Design of Pre-filter 2

Pre-filter 2 is derived from (13) and is given by:

$$\hat{r}_{I,i} = \frac{\mathcal{N}_i(p)\mathcal{G}_i}{a(p)} \sum_{k=1}^m \mathbb{B}_{ik}\hat{I}_{k,h}, \quad (16)$$

where the input consists of the aggregate estimates of fault-free line currents, the output $\hat{r}_{I,i}$ represents the estimated contribution of $\sum_{k=1}^m \mathbb{B}_{ik}I_{k,h}$ to r_i . According to (13), (15), and (16), the

residual \tilde{r}_i in Fig. 3 encapsulating the information of $f_{I,i}$ and P_i is then generated by subtracting $\hat{r}_{I,i}$ from r_i , yielding

$$\begin{aligned}\tilde{r}_i &= r_i - \frac{\mathcal{N}_i(p)\mathcal{G}_i}{a(p)} \sum_{k=1}^m \mathbb{B}_{ik} \hat{I}_{k,h} \\ &= \frac{\mathcal{N}_i(p)\mathcal{G}_i}{a(p)} \left(f_{I,i} + \frac{P_i}{V_i} \right) + \frac{\mathcal{N}_i(p)[\mathcal{G}_i \mathbf{I}_6]}{a(p)} \begin{bmatrix} \sum_{k=1}^m \mathbb{B}_{ik} \epsilon_k \\ \omega_i \end{bmatrix},\end{aligned}\quad (17)$$

where the aggregate faulty line current $f_{I,i} = \sum_{k=1}^m \mathbb{B}_{ik} I_{k,f}$ as previously defined. To facilitate the subsequent estimation process, we further transform the second line of (17) into its corresponding observable canonical state-space form:

$$\begin{cases} \dot{x}_{\tilde{r}_i}(t) = A_r x_{\tilde{r}_i}(t) + B_{\mathcal{G},i} \left(f_{I,i}(t) + \frac{P_i(t)}{V_i(t)} \right) + B_{\varpi,i} \varpi_i(t), \\ \tilde{r}_i(t) = C_r x_{\tilde{r}_i}(t), \end{cases}\quad (18)$$

where $x_{\tilde{r}_i}(t) \in \mathbb{R}^{d_{\mathcal{N}}+1}$ and $\varpi_i = [\sum_{k=1}^m \mathbb{B}_{ik} \epsilon_k \quad \omega_i]^\top$. Matrices A_r and C_r are specified in (9), the input matrices $B_{\mathcal{G},i}$ and $B_{\varpi,i}$ are constructed as:

$$B_{\mathcal{G},i} = \begin{bmatrix} \mathcal{N}_{i,0}^\top & \mathcal{N}_{i,1}^\top & \dots & \mathcal{N}_{i,d_{\mathcal{N}}}^\top \end{bmatrix}^\top \mathcal{G}_i, \quad B_{\varpi,i} = \begin{bmatrix} \mathcal{N}_{i,0}^\top & \mathcal{N}_{i,1}^\top & \dots & \mathcal{N}_{i,d_{\mathcal{N}}}^\top \end{bmatrix}^\top [\mathcal{G}_i \quad \mathbf{I}_6].$$

4.4. Design of Faulty Line Current Estimator

The three sub-blocks designed above serve as preparatory steps for estimating $f_{I,i}$. As illustrated in Fig. 3, the derived \tilde{r}_i is processed by the estimator in the final sub-block to compute $\hat{f}_{I,i}$. In this final stage, a discrete-time estimation approach is developed, and thus the state-space model (18) is discretized with a sampling period t_s . For consistency and simplicity, the system matrix notations of the discrete-time model remain unchanged. To address the potential ill-posedness issue in estimating $f_{I,i}$ mentioned in the problem statement session, the proposed approach proceeds through two sequential phases:

- (1) **Detection and differentiation phase.** Before any power line faults, i.e., $f_{I,i} = 0$, a residual $\tilde{\mathbf{Y}}_{i,T}$ derived from the estimate of P_i is introduced to detect both step load changes and power line faults. The discrimination between the two events is further achieved by leveraging their unique transient signatures in the residual signal $\tilde{\mathbf{Y}}_{i,T}$.
- (2) **Estimation phase.** Once a power line fault is detected, a dedicated estimator is activated to estimate $f_{I,i}$.

The methodologies employed in each phase are elaborated in the remaining parts of this subsection.

4.4.1. Detection and differentiation of power line faults and step load changes

The proposed detection and differentiation approach relies on power load estimation before faults occur on the power lines connected to DG unit i . Suppose that $f_{I,i} = 0$ and P_i is constant initially. To obtain power load estimation, we construct the following parity-space relation over a sliding window T based on (18):

$$\tilde{\mathbf{r}}_{i,T}(k) = \mathcal{O}_{i,T} x_{\tilde{r}_i}(k-T+1) + \mathcal{Z}_{i1,T} \mathbf{V}_{i,T-1}(k-1) P_i + \mathcal{Z}_{i2,T} \varpi_{i,T-1}(k-1), \quad (19)$$

where $\tilde{\mathbf{r}}_{i,T}(k)$, $\mathbf{V}_{i,T-1}(k-1)$, and $\varpi_{i,T-1}(k-1)$ are the stacked data vectors of \tilde{r}_i , $1/V_i$, and ϖ_i , respectively. Toeplitz matrices $\mathcal{Z}_{i1,T}$, $\mathcal{Z}_{i2,T}$, and the T -order observability matrix $\mathcal{O}_{i,T}$ are defined

as:

$$\mathcal{Z}_{i_1,T} = \begin{bmatrix} 0 & 0 & \dots & 0 \\ C_r B_{\mathcal{G},i} & 0 & \dots & 0 \\ C_r A_r B_{\mathcal{G},i} & C_r B_{\mathcal{G},i} & \dots & 0 \\ \vdots & \ddots & \ddots & \vdots \\ C_r A_r^{T-2} B_{\mathcal{G},i} & \dots & \dots & C_r B_{\mathcal{G},i} \end{bmatrix}, \quad \mathcal{Z}_{i_2,T} = \begin{bmatrix} 0 & 0 & \dots & 0 \\ C_r B_{\varpi,i} & 0 & \dots & 0 \\ C_r A_r B_{\varpi,i} & C_r B_{\varpi,i} & \dots & 0 \\ \vdots & \ddots & \ddots & \vdots \\ C_r A_r^{T-2} B_{\varpi,i} & \dots & \dots & C_r B_{\varpi,i} \end{bmatrix},$$

$$\mathcal{O}_{i,T} = [C_r^\top \quad (C_r A_r)^\top \quad \dots \quad (C_r A_r^{T-1})^\top]^\top.$$

To simplify the subsequent analysis, we further introduce the orthogonal projection of $\mathcal{O}_{i,T}$, i.e., $\mathcal{O}_{i,T}^\perp = I - \mathcal{O}_{i,T} \mathcal{O}_{i,T}^\dagger$. Multiplying both sides of (19) from the left by $\mathcal{O}_{i,T}^\perp$ leads to

$$\Upsilon_{i,T}(k) = \Psi_{i,T}(k-1)P_i + \Omega_{i,T}(k-1), \quad (20)$$

where $\Upsilon_{i,T}(k) = \mathcal{O}_{i,T}^\perp \tilde{\mathbf{r}}_{i,T}(k) \in \mathbb{R}^{n_\Upsilon}$, $\Psi_{i,T}(k-1) = \mathcal{O}_{i,T}^\perp \mathcal{Z}_{i_1,T} \mathbf{V}_{i,T-1}(k-1)$, and $\Omega_{i,T}(k-1) = \mathcal{O}_{i,T}^\perp \mathcal{Z}_{i_2,T} \boldsymbol{\varpi}_{i,T-1}(k-1)$. For notational simplicity, the time index is omitted hereafter, e.g., $\Upsilon_{i,T}(k) \rightarrow \Upsilon_{i,T}$.

Given (20), the weighted least-squares method is employed here to estimate P_i . The estimated value \hat{P}_i is given by

$$\hat{P}_i = \arg \min_{P_i} \|\Upsilon_{i,T} - \Psi_{i,T} P_i\|_{\Sigma_{\Omega_{i,T}}^{-1}}^2 = \Phi_{i,T} \Upsilon_{i,T}, \quad (21)$$

where $\Phi_{i,T} = (\Psi_{i,T}^\top \Sigma_{\Omega_{i,T}}^{-1} \Psi_{i,T})^{-1} \Psi_{i,T}^\top \Sigma_{\Omega_{i,T}}^{-1}$ and $\Sigma_{\Omega_{i,T}} = \mathcal{O}_{i,T}^\perp \mathcal{Z}_{i_2,T} \Sigma_{\boldsymbol{\varpi}_{i,T-1}} (\mathcal{O}_{i,T}^\perp \mathcal{Z}_{i_2,T})^\top \succ 0$ represents the covariance matrix of $\Omega_{i,T}$.

To detect load changes or power line faults, the following residual is introduced:

$$\tilde{\Upsilon}_{i,T} = \Upsilon_{i,T} - \Psi_{i,T} \hat{P}_i, \quad (22)$$

where the κ -th row of $\tilde{\Upsilon}_{i,T}$ is $\tilde{\Upsilon}_{i,T}^{[\kappa]} = \Upsilon_{i,T}^{[\kappa]} - \Psi_{i,T}^{[\kappa]} \hat{P}_i$, $\kappa \in \{1, \dots, n_\Upsilon\}$. Note that when there are no load changes and line faults, \hat{P}_i obtained from (21) is the minimum-variance unbiased estimate of P_i [34, Section 4.5]. Therefore, we have

$$\mathbf{E} [\tilde{\Upsilon}_{i,T}^{[\kappa]}] = 0, \quad \mathbf{Var} [\tilde{\Upsilon}_{i,T}^{[\kappa]}] = e_\kappa (\mathbf{I}_{n_\Upsilon} - \Psi_{i,T} \Phi_{i,T}) \Sigma_{\Omega_{i,T}} e_\kappa^\top,$$

where e_κ is a row vector with all entries zero except for the κ -th entry being 1. According to Chebyshev's inequality, in the absence of load changes and power line faults, the probability that $\tilde{\Upsilon}_{i,T}^{[\kappa]}(k)$ lies inside the threshold interval $[-\varepsilon_i^{[\kappa]}(k), \varepsilon_i^{[\kappa]}(k)]$ satisfies:

$$\mathbf{Pr} \left[\left| \tilde{\Upsilon}_{i,T}^{[\kappa]}(k) \right| \leq \varepsilon_i^{[\kappa]}(k) \mid \Delta P_i = 0, \mathbf{f}_{I,T-1} = \mathbf{0} \right] \geq 1 - \frac{1}{\alpha^2},$$

where ΔP_i denotes the step load change, $\mathbf{f}_{I,T-1}$ is the stacked data vector of $f_{I,i}$, $\alpha > 1$ is a tunable scalar, and the time-varying bound is $\varepsilon_i^{[\kappa]}(k) = \alpha \sqrt{\mathbf{Var} [\tilde{\Upsilon}_{i,T}^{[\kappa]}(k)]}$.

Based on the above analysis, deviations caused by both load changes and line faults can be detected if any entries in $\tilde{\Upsilon}_{i,T}$ exceed the pre-defined threshold interval. Moreover, we show in the following proposition that $\tilde{\Upsilon}_{i,T}$ exhibits distinct transient behaviors under these two scenarios, which serves as the foundation for distinguishing between step load changes and power line faults.

Proposition 4.1 (Discrimination between step load changes and power line faults). *Consider the power line dynamics (2), the closed-loop dynamics of DG unit i (4), and Assumptions 2.3 and 2.4. Suppose that load changes and line faults do not occur simultaneously within the sliding window T .*

The residual $\tilde{\mathbf{Y}}_{i,T}$ in (22), generated through the diagnosis block $\mathcal{D}_{l,i}$, exhibits distinct patterns under the two scenarios of step load changes and power line faults, as follows:

- (1) **Step load changes in P_i .** Entries in $\tilde{\mathbf{Y}}_{i,T}$ can temporarily exceed the threshold interval $[-\varepsilon_i^{[\kappa]}(k), \varepsilon_i^{[\kappa]}(k)]$ under the effect of step load changes. Then, with probability greater than $1 - 1/\alpha^2$, the entries return to and remain within the threshold bounds after T steps following the load changes.
- (2) **Power line faults on DG unit i .** The expected value of $\tilde{\mathbf{Y}}_{i,T}^{[\kappa]}$ in the presence of $f_{I,i}$ becomes

$$\mathbf{E} [\tilde{\mathbf{Y}}_{i,T}^{[\kappa]}] = e_\kappa (\mathbf{I}_{n_\Upsilon} - \Psi_{i,T} \Phi_{i,T}) \mathcal{O}_{i,T}^\perp \mathcal{Z}_{i,T} \mathbf{f}_{I,i,T-1},$$

and the faults can be distinguished from step changes in P_i if there consistently exists at least one entry in $\tilde{\mathbf{Y}}_{i,T}(k)$ that satisfies $\tilde{\mathbf{Y}}_{i,T}^{[\kappa]}(k) \notin [-\varepsilon_i^{[\kappa]}(k), \varepsilon_i^{[\kappa]}(k)]$ for at least T consecutive steps.

Proof. The proof is relegated to Appendix A. □

According to Proposition 4.1, step load changes and power line faults can be distinguished by evaluating the duration of their effects on $\tilde{\mathbf{Y}}_{i,T}$. To calculate the duration time during which not all $\tilde{\mathbf{Y}}_{i,T}^{[\kappa]}$ remain within the threshold intervals, we introduce $\mathcal{T}_i(k)$ to record the most recent time instant at which all $\tilde{\mathbf{Y}}_{i,T}^{[\kappa]}$ are inside the thresholds, which is

$$\mathcal{T}_i(k) := \max \left\{ k' \in \mathbb{N} : \tilde{\mathbf{Y}}_{i,T}^{[\kappa]}(k') \in [-\varepsilon_i^{[\kappa]}(k'), \varepsilon_i^{[\kappa]}(k')], \forall \kappa \in \{1, \dots, n_\Upsilon\}, k \geq k' \right\}. \quad (23)$$

In other words, $k - \mathcal{T}_i(k)$ measures the time elapsed since there exists $\tilde{\mathbf{Y}}_{i,T}^{[\kappa]}$ crossing the thresholds. In addition, we define $\sigma_i(k) \in \{0, 1, 2\}$ as the status indicator, whose value is determined by the following rules:

- (1) **No load changes or power line faults** ($\sigma(k) = 0$). If $k - \mathcal{T}_i(k) < T/2$, then all entries of $\tilde{\mathbf{Y}}_{i,T}(k)$ are within their respective thresholds, i.e., $\tilde{\mathbf{Y}}_{i,T}^{[\kappa]}(k) \in [-\varepsilon_i^{[\kappa]}(k), \varepsilon_i^{[\kappa]}(k)], \forall \kappa \in \{1, \dots, n_\Upsilon\}$, or there exist entries of $\tilde{\mathbf{Y}}_{i,T}(k)$ exceeding thresholds while the duration is less than $T/2$. Note that some entries of $\tilde{\mathbf{Y}}_{i,T}(k)$ may transiently exceed the thresholds due to stochastic noise even without load changes and faults. To mitigate false alarms, we set $\sigma_i(k) = 0$ if threshold violations persist for less than a predefined duration, e.g., $T/2$ here;
- (2) **Step load changes or line faults** ($\sigma(k) = 1$). If $T/2 \leq k - \mathcal{T}_i(k) < T$, then there exists at least one element $\tilde{\mathbf{Y}}_{i,T}^{[\kappa]}(t) \notin [-\varepsilon_i^{[\kappa]}(t), \varepsilon_i^{[\kappa]}(t)]$ for each $t \in \{\mathcal{T}_i(k) + 1, \dots, k\}$ with duration less than T while larger than and equal to $T/2$;
- (3) **Persistent line faults** ($\sigma(k) = 2$). If $k - \mathcal{T}_i(k) \geq T$, then there exists $\kappa \in \{1, \dots, n_\Upsilon\}$ such that $\tilde{\mathbf{Y}}_{i,T}^{[\kappa]}(k) \notin [-\varepsilon_i^{[\kappa]}(k), \varepsilon_i^{[\kappa]}(k)]$ for at least T consecutive steps.

For clarity, the diagnosis rules are summarized as follows:

$$\sigma_i(k) = \begin{cases} 0, & \text{if } k - \mathcal{T}_i(k) < T/2, \\ 1, & \text{if } T/2 \leq k - \mathcal{T}_i(k) < T, \\ 2, & \text{if } k - \mathcal{T}_i(k) \geq T. \end{cases} \quad (24)$$

4.4.2. Estimation of aggregated faulty line current

Upon successful detection of any faulty line current $f_{I,i}$ in DG unit i , an estimator is activated. The design method of the estimator is provided in this part. We begin by reformulating the parity-space equation (20) based on (18) to account for power line faults and obtain:

$$\Upsilon_{i,T} = \mathcal{O}_{i,T}^\perp \mathcal{Z}_{i1,T} (\mathbf{V}_{i,T-1} P_i + \Delta \mathbf{P}_i + \mathbf{f}_{I,i,T-1}) + \Omega_{i,T}, \quad (25)$$

where $\Delta \mathbf{P}_i = \begin{bmatrix} \mathbf{0}^\top & \mathbf{V}_{i,k-k_0}^\top \end{bmatrix}^\top \Delta P_i$ represents the step load change occurring at $k_0 \in [k-T+1, k-1]$ and $\mathbf{f}_{I,i,T-1}$ is the stacked data vector of $f_{I,i}$. It is worth noting that $\mathcal{O}_{i,T}^\perp \mathcal{Z}_{i1,T} \mathbf{V}_{i,T-1}$ is a linear combination of columns of $\mathcal{O}_{i,T}^\perp \mathcal{Z}_{i1,T}$ and the following rank condition holds:

$$\text{Rank} \left(\begin{bmatrix} \mathcal{O}_{i,T}^\perp \mathcal{Z}_{i1,T} & \mathcal{O}_{i,T}^\perp \mathcal{Z}_{i1,T} \mathbf{V}_{i,T-1} \end{bmatrix} \right) = \text{Rank}(\mathcal{O}_{i,T}^\perp \mathcal{Z}_{i1,T}).$$

Consequently, P_i and $\mathbf{f}_{I,i,T-1}$ cannot be uniquely determined through (25). To address this issue, instead of directly estimating $\mathbf{f}_{I,i,T-1}$, we opt to estimate its mean value over the past $T-1$ steps, i.e.,

$$\mathbf{f}_{I,i,T-1} = \mathbf{1} \bar{f}_{I,i,T-1} + \Delta \mathbf{f}_{I,i,T-1},$$

where $\bar{f}_{I,i,T-1} = \frac{1}{T-1} \sum_{k=T+1}^{k-1} f_{I,i}(k')$ is the mean value, $\Delta \mathbf{f}_{I,i,T-1}$ represents the deviation, and $\mathbf{1} = [1 \dots 1]^\top$. Then, the parity-space relation (25) is reformulated as:

$$\Upsilon_{i,T} = \Gamma_{i,T} \Theta_i + \mathcal{O}_{i,T}^\perp \mathcal{Z}_{i1,T} (\Delta \mathbf{f}_{I,i,T-1} + \Delta \mathbf{P}_i) + \Omega_{i,T}. \quad (26)$$

where $\Gamma_{i,T} = \mathcal{O}_{i,T}^\perp \mathcal{Z}_{i1,T} [\mathbf{V}_{i,T-1} \mathbf{1}]$ and $\Theta_i = [P_i \bar{f}_{I,i,T-1}]^\top$.

In (26), $\text{Rank}(\Gamma_{i,T}) = 2$ is of full column rank as long as $\mathbf{V}_{i,T-1}$ is not a constant vector. Nevertheless, the estimate of Θ_i is still susceptible to load deviations $\Delta \mathbf{P}_i$, faulty current fluctuations $\Delta \mathbf{f}_{I,i,T-1}$, and noise term $\Omega_{i,T}$. This sensitivity stems from the ill-conditioning of $\Gamma_{i,T}$ when $\mathbf{V}_{i,T-1}$ exhibits near-constant behavior. Therefore, to estimate $\bar{f}_{I,i,T-1}$ robustly, we formulate the following regularized least-squares problem:

$$\hat{\Theta}_i = \arg \min_{\Theta_i} \|\Upsilon_{i,T} - \Gamma_{i,T} \Theta_i\|_{\Sigma_{\Omega_{i,T}}^{-1}}^2 + \eta \|\nu_1 (\Theta_i - \hat{\Theta}_{i-})\|_2^2, \quad (27)$$

where $\hat{\Theta}_i = [\hat{P}_i \hat{f}_{I,i}]^\top$ is the estimate of Θ_i , $\eta \in \mathbb{R}_+$ is the regularization weight, $\nu_1 = [1 \ 0]$ selectively penalizes variations in the load estimate, and $\hat{\Theta}_{i-}$ represents the estimation result from the previous time step. The regularization term enforces temporal consistency on P_i , reflecting its piece-wise constant nature in practical systems.

Although (27) is a quadratic optimization problem and can be solved tractably, it is not suitable for online monitoring as it requires solving the optimization problem at each step, which can be computationally expensive. Fortunately, (27) admits an analytical solution, as presented in the following proposition.

Proposition 4.2 (Analytical solution). *The analytical solution to the quadratic optimization problem (27) is given by*

$$\hat{\Theta}_i = \mathcal{K}_{i,T}^{-1} \left(\Gamma_{i,T}^\top \Sigma_{\Omega_{i,T}}^{-1} \Upsilon_{i,T} + \eta \nu_1^\top \nu_1 \hat{\Theta}_{i-} \right). \quad (28)$$

where $\mathcal{K}_{i,T} = \Gamma_{i,T}^\top \Sigma_{\Omega_{i,T}}^{-1} \Gamma_{i,T} + \eta \nu_1^\top \nu_1$. The estimate of $\bar{f}_{I,i,T-1}$ is obtained by $\hat{f}_{I,i} = \nu_2 \hat{\Theta}_i$ with $\nu_2 = [0 \ 1]$.

Proof. By defining the objective function in (27) as $J(\Theta_i)$ and taking the derivative of $J(\Theta_i)$ over Θ_i , we have

$$\frac{\partial J(\Theta_i)}{\partial \Theta_i} = 2 \left(\Gamma_{i,T}^\top \Sigma_{\Omega_{i,T}}^{-1} \Gamma_{i,T} + \eta \nu_1^\top \nu_1 \right) \Theta_i - 2 \left(\Gamma_{i,T}^\top \Sigma_{\Omega_{i,T}}^{-1} \Upsilon_{i,T} + \eta \nu_1^\top \nu_1 \hat{\Theta}_i \right).$$

The solution is obtained by setting $\partial J(\Theta_i)/\partial \Theta_i = 0$. This completes the proof. \square

The diagnosis processes of both actuator and power line faults in DG unit i are summarized in Algorithm 1. Furthermore, to facilitate the subsequent result about the performance bound of the estimator (28), some notations are introduced. Recall that $\Psi_{i,T} = \mathcal{O}_{i,T}^\perp \mathcal{Z}_{i_1,T} \mathbf{V}_{i,T-1}$ in (20). We further define $\bar{\mathcal{Z}}_{i,T} = \mathcal{O}_{i,T}^\perp \mathcal{Z}_{i_1,T} \mathbf{1}$, thus $\Gamma_{i,T}$ in (26) becomes $\Gamma_{i,T} = [\Psi_{i,T} \ \bar{\mathcal{Z}}_{i,T}]$. Let $\underline{\lambda}_{\Sigma_{\Omega_{i,T}}}$ and $\bar{\lambda}_{\Sigma_{\Omega_{i,T}}}$ denote the smallest and largest eigenvalues of $\Sigma_{\Omega_{i,T}}$, respectively. The following theorem provides a bound for the estimation error of the average value of $f_{I,i}$.

Theorem 4.3 (Performance bound of the regularized estimator). *Considering the power line dynamics (2), the closed-loop dynamics of DG unit i (4), and Assumptions 2.3 and 2.4, the estimated value $\hat{f}_{I,i}$ of $\bar{f}_{I,T-1}$ obtained from (28) through the diagnosis block $\mathcal{D}_{l,i}$, satisfies the following error bound:*

$$\begin{aligned} \left| \mathbf{E} \left[\bar{f}_{I,T-1} - \hat{f}_{I,i} \right] \right| &\leq \frac{\bar{\lambda}_{\Sigma_{\Omega_{i,T}}}}{\underline{\lambda}_{\mathcal{M}_{i,T}} + \eta \bar{\lambda}_{\Sigma_{\Omega_{i,T}}}} \frac{\sqrt{\bar{\lambda}_{\mathcal{M}_{i,T}}}}{\underline{\lambda}_{\Sigma_{\Omega_{i,T}}}} \bar{\sigma}(\mathcal{O}_{i,T}^\perp \mathcal{Z}_{i_1,T}) (\|\Delta \mathbf{f}_{I,T-1}\|_2 + \|\Delta \mathbf{P}_i\|_2) \\ &\quad + \frac{\bar{\lambda}_{\Sigma_{\Omega_{i,T}}} \bar{\mathcal{Z}}_{i,T}^\top \Psi_{i,T}}{\underline{\lambda}_{\Sigma_{\Omega_{i,T}}} \bar{\mathcal{Z}}_{i,T}^\top \bar{\mathcal{Z}}_{i,T}} |P_i - \hat{P}_i|, \end{aligned} \quad (29)$$

where $\bar{\lambda}_{\mathcal{M}_{i,T}} = \Psi_{i,T}^\top \Psi_{i,T} + \bar{\mathcal{Z}}_{i,T}^\top \bar{\mathcal{Z}}_{i,T}$ and $\underline{\lambda}_{\mathcal{M}_{i,T}} = \frac{\Psi_{i,T}^\top \Psi_{i,T} \bar{\mathcal{Z}}_{i,T}^\top \bar{\mathcal{Z}}_{i,T} - \Psi_{i,T}^\top \bar{\mathcal{Z}}_{i,T} \bar{\mathcal{Z}}_{i,T}^\top \Psi_{i,T}}{\Psi_{i,T}^\top \Psi_{i,T} + \bar{\mathcal{Z}}_{i,T}^\top \bar{\mathcal{Z}}_{i,T}}$.

Proof. The proof is relegated to Appendix B. \square

The bound in (29) holds for each time instant k after power line fault detection, and for simplicity, k is omitted here. Let us elaborate further on how different factors influence the bound:

- (1) **Ill-conditioning issue.** When $V_i(k)$ approaches a constant value, $\underline{\lambda}_{\mathcal{M}_{i,T}}$ in the denominator of (29) tends to zero. This makes the estimation problem ill-conditioned without the regularized term in (27), i.e., $\eta = 0$.
- (2) **Variation terms $\Delta \mathbf{f}_{I,T-1}$ and $\Delta \mathbf{P}_i$.** The bound is affected by the fault deviation $\Delta \mathbf{f}_{I,T-1}$ and the load change $\Delta \mathbf{P}_i$, whose effect can be mitigated effectively by choosing a large enough η .
- (3) **Priori estimation result \hat{P}_{i-} .** The regularization term in (27) enforces P_i to stay close to its prior estimate. Initially, $|P_i - \hat{P}_i|$ is small as the estimation result of P_i from differentiation phase (21) is unbiased. However, step changes in P_i during the estimation phase will increase the estimation error, which is explicitly reflected in the last term of (29). Moreover, as η approaches infinity, the error bound converges to the value determined by $|P_i - \hat{P}_{i-}|$.

Remark 4.4 (Selection of η). *The right-hand side of inequalities (29) indicates that increasing η in (27) can reduce the expectation of the estimation error. Therefore, a large enough η needs to be chosen to ensure estimation performance, while being numerically bounded for practical considerations.*

Algorithm 1 Fault diagnosis process for DG unit i

I. Estimation of the actuator fault $f_{a,i}$

- (a) Input Y_i to the estimation filter (6)
- (b) Output the estimated value $\hat{f}_{a,i}$

II. Estimation of the faulty line current $f_{I,i}$

- (a) *Initialization*: Choose the time window length T and initialize the iteration index $k = T$.
Set the status indicator $\sigma_i(k-1) = 0$ and the crossing time recorder $\mathcal{T}_i(k-1) = k-1$
 - (b) Generate \tilde{r}_i using pre-filter 1 in (12), line current estimators in (14), pre-filter 2 in (16), and (18)
 - (c) Generate $\Upsilon_{i,T} = \mathcal{O}_{i,T}^\perp \tilde{r}_{i,T}$ in (20) with discretized \tilde{r}_i
 - (d) Compute the covariance matrix $\Omega_{i,T}$
 - (e) If $\sigma_i(k-1) = 0$ or $\sigma_i(k-1) = 1$ % Fault-load discrimination phase:
 - $\hat{P}_i = \Phi_{i,T} \Upsilon_{i,T}$ in (21);
 - $\tilde{\Upsilon}_{i,T} = \Upsilon_{i,T} - \Psi_{i,T} \hat{P}_i$ in (22);
 - If $\exists \tilde{\Upsilon}_{i,T}^{[\kappa]} \notin [-\varepsilon_i^{[\kappa]}(k), \varepsilon_i^{[\kappa]}(k)]$
 - $\mathcal{T}_i(k) = \mathcal{T}_i(k-1)$; % Record crossing time
 - Else
 - $\mathcal{T}_i(k) = k$;
 - End
 - Use the diagnosis rules (24) to determine the current value of the indicator $\sigma_i(k)$;
 - (f) Else %Estimation phase:
 - Generate the estimated value $\hat{\Theta}_i$ using (28);
 - Set $\sigma_i(k) = 2$;
 - (g) End
 - (h) Set $k = k + 1$ and repeat (b)-(h).
-

Remark 4.5 (Location of the faulty line). *Faults on a power line can be detected and estimated by the diagnosis components of the DG units located at both ends of the line. By analyzing the estimated faulty line currents, the faulty line can be identified in some scenarios. For instance, in the simplest case where only one line in the DC microgrid is faulty, the fault location can be precisely determined.*

Remark 4.6 (Conservativeness analysis). *While the regularization term introduced in (27) resolves the issue of the matrix $\Gamma_{i,T}$ being close to singularity, it restricts the variation of the estimate of P_i relative to its previous value. Consequently, the proposed estimation approach exhibits limited accuracy in estimating step load changes during the estimation phase. Nevertheless, the estimation performance for faulty line current $f_{I,i}$ improves by increasing the value of η as discussed above. Moreover, we observed in the simulation results that the impact of load changes on the estimation of $f_{I,i}$ is limited.*

5. SIMULATION RESULTS

In this section, the effectiveness of the proposed diagnosis scheme is validated on the DC microgrid depicted in Fig. 1, a simplified structure derived from [35]. The parameters of the microgrid are provided in Table 1, with the reference voltages set as $V_1^* = 48$ V, $V_2^* = 48.1$ V, and $V_3^* = 47.5$ V. Suppose that the microgrid is initially working under normal conditions. Then, faults might occur

TABLE 1. Parameters of the DC microgrid system.

Name	Values	Name	Values
$R_{t,1}$	0.2Ω	$L_{t,1}$	1.8 mH
$R_{t,2}$	0.3Ω	$L_{t,2}$	2 mH
$R_{t,3}$	0.1Ω	$L_{t,3}$	2.2 mH
$C_{t,1}$	2.21 mF	R_1	0.05Ω
$C_{t,2}$	1.9 mF	R_2	0.07Ω
$C_{t,3}$	1.7 mF	L_1	$2.1 \mu\text{F}$
K_1	$[-15 \ -2 \ 70]^\top$	L_2	$1.8 \mu\text{F}$
K_2	$[-15 \ -2 \ 50]^\top$	K_3	$[-15 \ -2 \ 50]^\top$

when the system is at or close to steady state. The initial conditions are thus set as $x_1(0) = [47.80, 6.93, 11.19]^\top$, $x_2(0) = [48.10, 4.76, 15.61]^\top$, and $x_3(0) = [47.50, -4.29, 15.02]^\top$. Additionally, since a discretization approach is employed to estimate the faulty current $f_{I,i}$, all simulation results are presented using sampling data to ensure consistency, with a sampling time of 1×10^{-5} s. Based on the above setup, the diagnosis performance of $\mathcal{D}_{a,i}$ and $\mathcal{D}_{l,i}$ is evaluated separately in the subsequent subsections.

5.1. Actuator Fault Diagnosis Results

To estimate actuator faults, an estimator $\mathcal{D}_{a,i}$ for each DG unit is designed by utilizing the approach proposed in Section 3. Taking $\mathcal{D}_{a,1}$ as an example, the design process is outlined as follows:

Step 1. Determine the degree and denominator of the filter in (6). For this example, the degree is $d_N = 2$, and the denominator is chosen as $a(p) = (0.5 + p)(0.1 + p)(1 + p)$.

Step 2. Obtain the parameters of the filter's numerator by solving the optimization problem (10) with the YALMIP toolbox [36].

Step 3. Construct the filter in (6). The estimation of $f_{a,1}$ can be generated by processing the locally available signals y_1 and V_1^* through the designed filter.

Suppose an incipient fault $f_{a,1}$ occurs in the voltage controller of DG 1 and a step fault $f_{a,3}$ occurs in the voltage controller of DG 3. The incipient fault $f_{a,1}(t) = 0$ for $t \leq 100$ ms, and for $t \geq 100$ ms, $f_{a,1}(t)$ evolves as:

$$\dot{f}_{a,1}(t) = -\beta_a f_{a,1}(t) + \beta_a \bar{f}_{a,1},$$

where $\beta_a = 8 \times 10^{-9}$ determines the changing rate and stealthiness of $f_{a,1}$ and $\bar{f}_{a,1} = 5$ is the final value of $f_{a,1}$. The step fault $f_{a,3}$ remains 0 until $t = 70$ ms, after which it becomes 0.5, i.e., $f_{a,3}(t) = 0.5$ for $t > 70$ ms.

To demonstrate that the designed estimator can decouple the effects of load changes and power line faults, we consider a step change in P_1 , i.e., $P_1(t) = 100$ W for $t \leq 40$ ms and $P_1(t) = 120$ W for $t > 40$ ms, as well as the occurrence of a power line fault between DG 1 and DG 2, i.e., $f_{L,1}(t) = 0$ for $t \leq 80$ ms and $f_{L,1}(t) = 0.1$ for $t > 80$ ms. The power load P_2 changes from 125 W to 110 W at 120 ms, and $P_3(t) = 140$ W is constant. Moreover, noise δ_i and ζ_i for $i = \{1, 2, 3\}$, ϵ_k for $k = \{1, 2\}$ are zero mean white noise with standard deviations 0.01, 0.001, and 0.01, respectively.

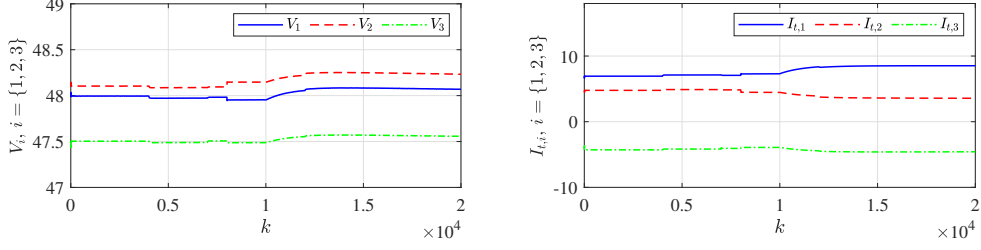


FIGURE 4. Dynamic response of the DC microgrid when considering $f_{a,1}$, $f_{a,3}$, $f_{L,1}$, and load changes.

The actuator fault estimation results are presented in Fig. 4 and Fig. 5. Specifically, Fig. 4 depicts the voltage and current variations within the microgrid in response to load changes and system faults. As can be seen that the measured signals V_i and $I_{t,i}$ do not provide clear indications of fault occurrences. Fig. 5 shows the diagnosis results from each local actuator fault estimator. For brevity, we just analyze the diagnosis results of $\mathcal{D}_{a,1}$ in Fig. 5(a), as the remaining results follow a similar analysis procedure. The first two subplots of Fig. 5(a) illustrate the load change in P_1 and the faulty current $f_{I,1}$, while the third subplot presents the actuator fault $f_{a,1}$ and its estimate $\hat{f}_{a,1}$. It can be observed that the estimated value $\hat{f}_{a,1}$ accurately follows the true fault signal $f_{a,1}$ and remains unaffected by load changes, power line faults, and neighboring DG unit dynamics.

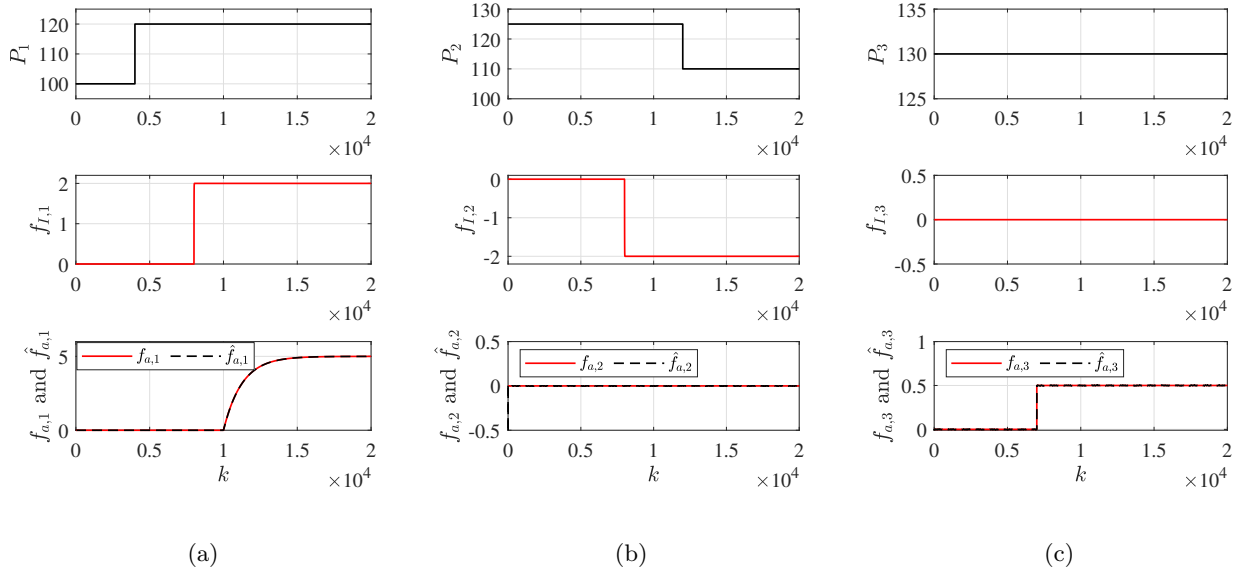


FIGURE 5. Diagnosis of actuator faults: (a) diagnosis results of $\mathcal{D}_{a,1}$, (b) diagnosis results of $\mathcal{D}_{a,2}$, and (c) diagnosis results of $\mathcal{D}_{a,3}$.

5.2. Power Line Fault Diagnosis Results

For the estimation of faulty line current $f_{I,i}$ induced by power line faults, we introduce the block $\mathcal{D}_{l,i}$ for each DG unit, whose structure is illustrated in Fig. 3. The proposed estimation scheme is compared with the multiple fault estimation method developed in [30] to demonstrate the superiority. Taking $\mathcal{D}_{l,1}$ as an example, its design process is summarized as follows:

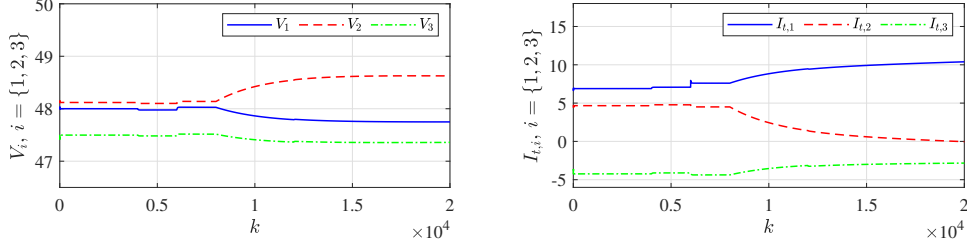


FIGURE 6. Dynamic response of the DC microgrid when considering the incipient power line fault.

Step 1. Design Pre-filter 1 depicted by (12) in Section 4.A. We choose the degree $d_{\mathcal{N}} = 2$ and the denominator $a(p) = (0.5 + p)(0.1 + p)(1 + p)$. The coefficients of $\mathcal{N}_1(p)$ are determined using the approach outlined in Proposition 3.1. The residual generator (12) takes locally available signals y_1 and V_1^* as inputs and produces the output r_1 .

Step 2. Design line current estimators described by (14) in Section 4.B for all power lines connected to DG 1. These line current estimators use the PCC voltages at the ends of the power lines (i.e., V_1, V_2 , and V_3 for DG 1) as inputs and generate the estimated fault-free component of the line currents $\hat{I}_{1,h}$ and $\hat{I}_{2,h}$.

Step 3. Design Pre-filter 2 described by (16) in Section 4.C and generate the residual \tilde{r}_1 used for faulty line current estimation. The input of Pre-filter 2 is the sum of the estimated healthy line currents $\hat{I}_{1,h}$ and $\hat{I}_{2,h}$. Then, the residual \tilde{r}_1 can be obtained based on (17).

Step 4. Design the faulty line current estimator for $f_{I,1}$ based on (26)-(28). Discretize the system with a sampling time of 1×10^{-5} s and choose a sliding window length of $T = 20$. The residual \tilde{r}_1 is first used to distinguish between step load changes and power line faults according to Proposition 4.1. The estimator (28) is activated when a power line fault is detected with the weight $\eta = 1 \times 10^6$, which produces the estimate of $\bar{f}_{I,1,T-1}$.

To verify the performance of the designed faulty current estimator $\mathcal{D}_{l,i}$, we consider two types of line faults: the incipient fault and the pole-to-ground short-circuit fault.

Case I: Incipient fault on power line 1. In the first scenario, we consider an incipient fault occurring on the power line between DG 1 and DG 2. The incipient power line fault $f_{L,1}(t) = 0$ for $t \leq 80$ ms, and for $t > 80$ ms, its dynamics become:

$$\dot{f}_{L,1}(t) = -\beta_l f_{L,1}(t) + \beta_l \bar{f}_{L,1},$$

where $\beta_l = 4 \times 10^{-9}$ and $\bar{f}_{L,1} = 1$. To further evaluate the decoupling capability of $\mathcal{D}_{l,1}$, an actuator fault $f_{a,1}$ is considered in DG 1, which is modeled as a step signal, i.e., $f_{a,1}(t) = 0$ for $t \leq 60$ ms and $f_{a,1}(t) = 2$ for $t > 60$ ms. Step changes in P_1 and P_3 are considered, i.e., $P_1(t)$ changes from 100 W to 120 W at $t = 40$ ms and $P_3(t)$ changes from 140 W to 130 W at $t = 120$ ms. The load of DG 2 remains constant at $P_2(t) = 110$ W.

Figs. 6-8 present the diagnosis results of the incipient power line fault $f_{L,1}$. Particularly, Fig. 6 illustrates the voltage and current variations of each DG unit under load changes and system faults. Due to the stealthiness of the fault, the occurrence of $f_{L,1}$ cannot be discerned directly from these measurements. Fig. 7 depicts the diagnosis result of the faulty line current estimator of each DG unit. For instance, Fig. 7(a) shows the results of $\mathcal{D}_{l,1}$. At $t = 40$ ms, the step change in P_1 is detected according to the diagnosis rules in (24), as the status indicator σ_1 (the third subfigure)

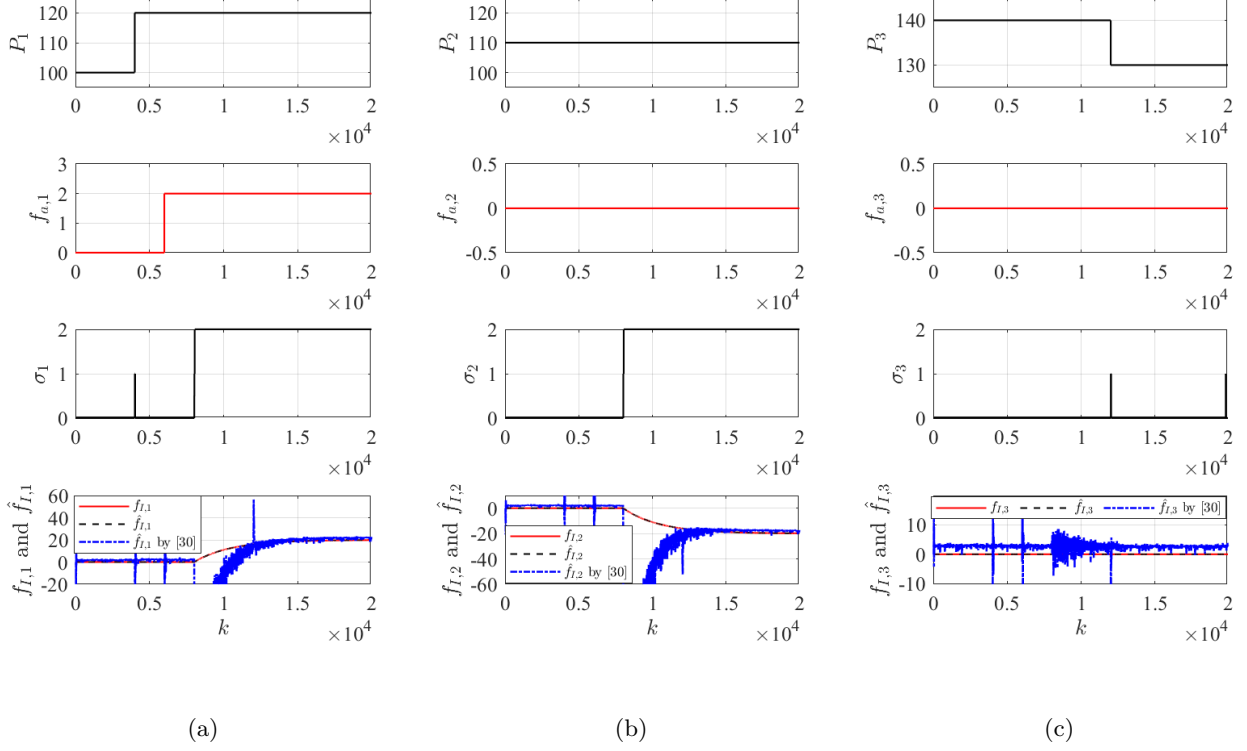


FIGURE 7. Diagnosis of incipient power line faults: (a) diagnosis results of $\mathcal{D}_{l,1}$, (b) diagnosis results of $\mathcal{D}_{l,2}$, and (c) diagnosis results of $\mathcal{D}_{l,3}$.

briefly switch to 1 with a duration shorter than the sliding window length T . At $t = 80$ ms, the fault $f_{L,1}$ happens and σ_1 becomes 2, meaning the successful detection of the power line fault $f_{L,1}$.

The bottom sub-figure of Fig. 7(a) compares the estimated values of the faulty current $f_{l,1}$ induced by $f_{L,1}$ using the proposed approach and that in [30]. As can be seen, the proposed estimation approach tracks the faulty current well, while the method in [30] exhibits significant estimation errors and oscillations due to the near-singularity problem. Note that the actuator fault $f_{a,1}$ and dynamics of other DG units have no effects on the diagnosis results of $\mathcal{D}_{l,1}$. Additionally, the power line fault $f_{L,1}$ is also detected and estimated by $\mathcal{D}_{l,2}$, as shown in Fig. 7(b). Fig. 8 shows the value $|\mathbf{E}[\bar{f}_{l,1,T-1} - \hat{f}_{l,1}]|$ and its upper bound given in (29). As the faulty current gradually converges to a constant, the upper bound of the error also decreases, which aligns well with the theoretical analysis.

Case II: Faults on both power lines 1 and 2. In the second scenario, we consider a more complex case, where the pole-to-ground short-circuit fault $f_{L,1}$ happens on the power line between DG 1 and DG 2, along with an incipient fault $f_{L,2}$ on the power line between DG 1 and DG 3. The equivalent circuit of the short-circuit fault is depicted in Fig. 9, with the dynamics described by:

$$\begin{cases} \dot{I}_k(t) = -\frac{R_{k,1}}{L_{k,1}}I_k(t) + \frac{1}{L_{k,1}}(V_i(t) - V_f(t)) \\ \dot{\tilde{I}}_k(t) = -\frac{R_{k,2}}{L_{k,2}}\tilde{I}_k(t) + \frac{1}{L_{k,2}}(V_f(t) - V_j(t)) \\ V_f(t) = (I_k(t) - \tilde{I}_k(t))R_f \end{cases}, \quad (30)$$

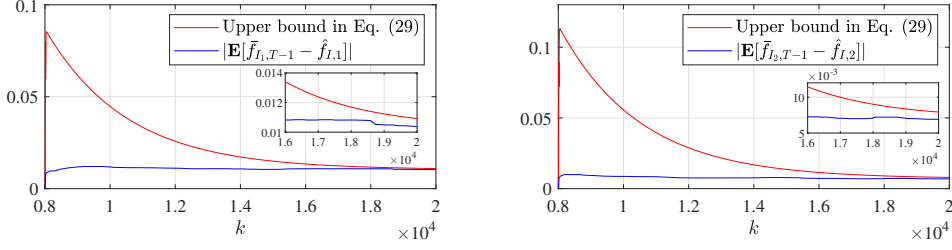


FIGURE 8. Performance bounds derived by Theorem 4.3.

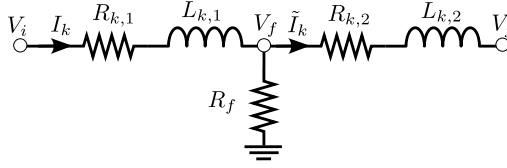


FIGURE 9. Illustration of the short-circuit fault.

where $k = 1$ and R_f is a low-resistance grounding resistor. Other inductance and resistance values depend on the short-circuit fault location. The dynamics of I_k can be rewritten in the form of (2), where the power line fault $f_{L,k}$ becomes

$$f_{L,k}(t) = \left(\frac{R_k}{L_k} - \frac{R_{k,1}}{L_{k,1}} \right) I_k(t) + \frac{1}{L_k} V_j(t) - \frac{1}{L_{k,1}} V_f(t).$$

The parameters in the circuit are $R_{k,1} = R_{k,2} = 0.025 \, \Omega$, $L_{k,1} = L_{k,2} = 1 \, \mu\text{H}$, and $R_f = 0.01 \, \Omega$. The short-circuit fault happens at $t = 100 \, \text{ms}$. The dynamics of the incipient fault $f_{L,2}$ follow: $\dot{f}_{L,2}(t) = -\beta_l f_{L,2}(t) + \beta_l \bar{f}_{L,2}$, with $\beta_l = 4 \times 10^{-9}$, $\bar{f}_{L,2} = 1$, and the occurrence time $t = 60 \, \text{ms}$. An actuator fault $f_{a,1}$ is considered in DG unit 1, which is described by a step signal and changes from 0 to 0.6 at $t = 100 \, \text{ms}$. Additionally, to assess the impact of load variations on faulty current estimation, we introduce a step change in P_2 , which decreases from 115 W to 105 W at $t = 150 \, \text{ms}$.

The simulation results of the second scenario are presented in Figs. 11-13. In particular, Fig. 11 shows the voltage and current variations of the microgrid under load changes and system faults. When the incipient power line fault $f_{L,2}$ happens, its effect on voltages and currents is unobvious from the measurements. In contrast, the short-circuit fault $f_{L,1}$ at $t = 100 \, \text{ms}$ introduces a low-resistance R_f , causing sharp voltage and current increases in the microgrid, as shown in Fig. 11. As a result, the short-circuit fault is easily detectable from measurement signals. Nevertheless, the proposed diagnosis approach can provide more detailed information about these faults.

The diagnosis results for the power line faults $f_{L,1}$ and $f_{L,2}$ are shown in Fig. 10. Specifically, at $t = 40 \, \text{ms}$, the status indicator σ_1 briefly switches to 1, indicating the detection of the step change in P_1 . At $t = 60 \, \text{ms}$, the incipient fault $f_{L,2}$ happens on the power line between DG units 1 and 3, then the indicator signals σ_1 and σ_3 switch to 2. This means that $f_{L,2}$ is detected by both $\mathcal{D}_{l,1}$ and $\mathcal{D}_{l,3}$. At $t = 100 \, \text{ms}$, the short-circuit fault $f_{L,1}$ between DG units 1 and 2 occurs, and the indicator signal σ_2 becomes 2, indicating successful detection of $f_{L,1}$. Note that the detection process is further supported by the residual behavior in Fig. 12. Due to the space limitation, we only show the residual $\tilde{Y}_{1,T}$ here.

The bottom row of Fig. 10 shows estimates of faulty line currents in each DG unit caused by $f_{L,1}$ and $f_{L,2}$. It can be seen that, faulty currents $f_{I,1}$ and $f_{I,3}$ caused by the incipient fault $f_{L,2}$ can

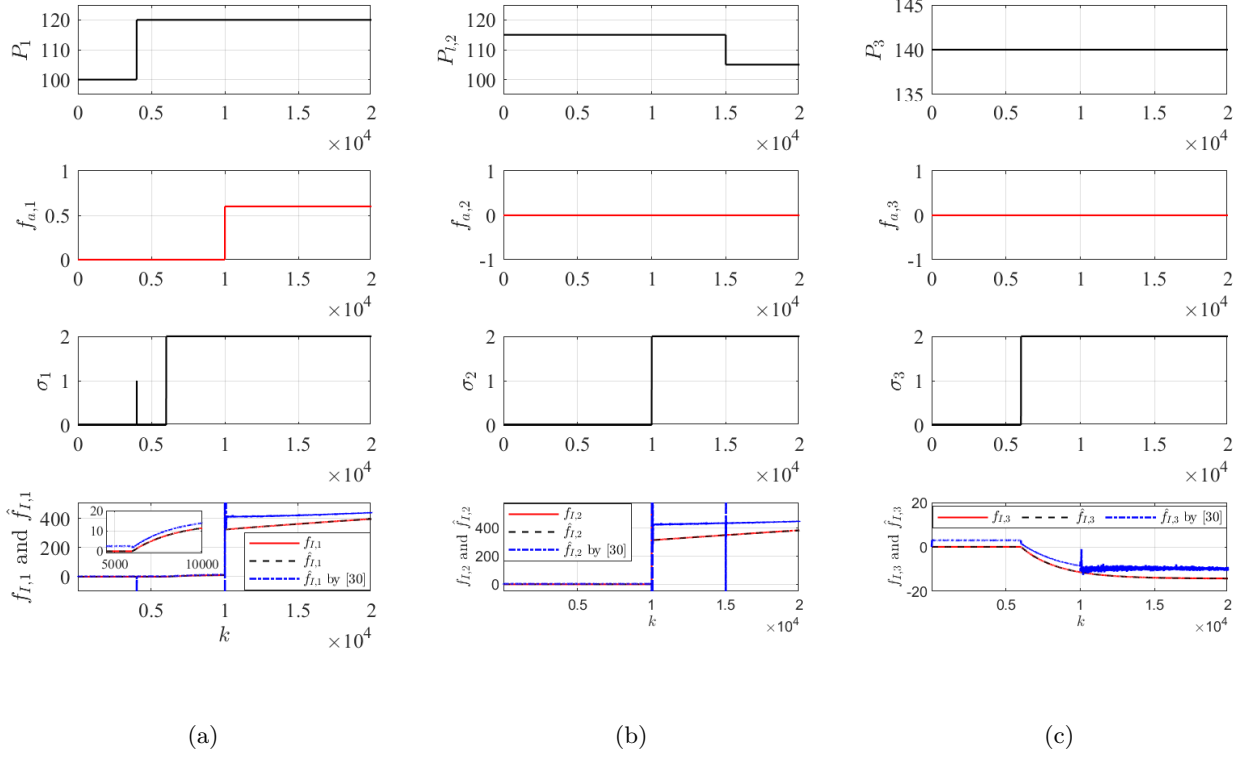


FIGURE 10. Diagnosis of short-circuit line faults: (a) diagnosis results of $\mathcal{D}_{l,1}$, (b) diagnosis results of $\mathcal{D}_{l,2}$, and (c) diagnosis results of $\mathcal{D}_{l,3}$.

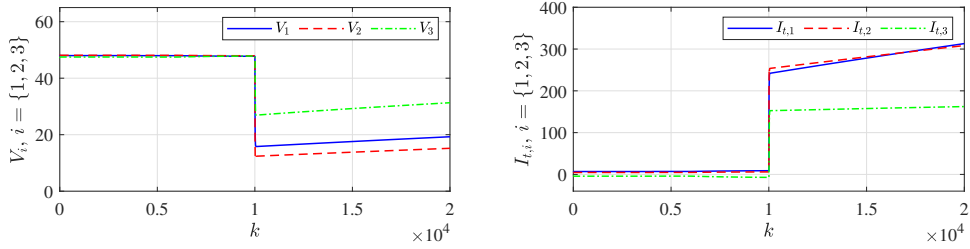


FIGURE 11. Dynamic response of the DC microgrid when considering the incipient and short-circuit line faults.

be accurately estimated by $\mathcal{D}_{l,1}$ and $\mathcal{D}_{l,3}$, respectively. After the short-circuit fault $f_{L,1}$ happens at $t = 100$ ms, the faulty current $f_{L,2}$ is estimated by $\mathcal{D}_{l,2}$, while $\mathcal{D}_{l,1}$ provides a combined estimate of currents from both $f_{L,1}$ and $f_{L,2}$. The comparison with the estimation method in [30] also shows the superiority of the proposed approach. Finally, Fig. 13 validates the developed upper bound on the estimation error in this scenario.

6. CONCLUSIONS

This paper presents a distributed diagnosis scheme for the detection and estimation of actuator and power line faults in DC microgrids, under the effects of unknown power loads and stochastic

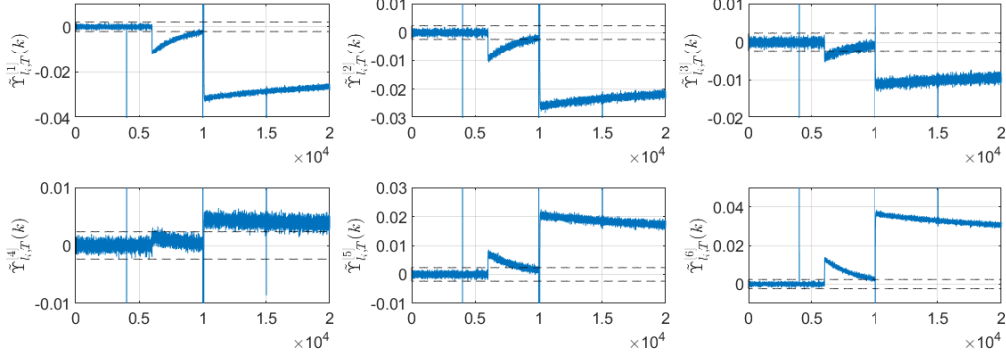
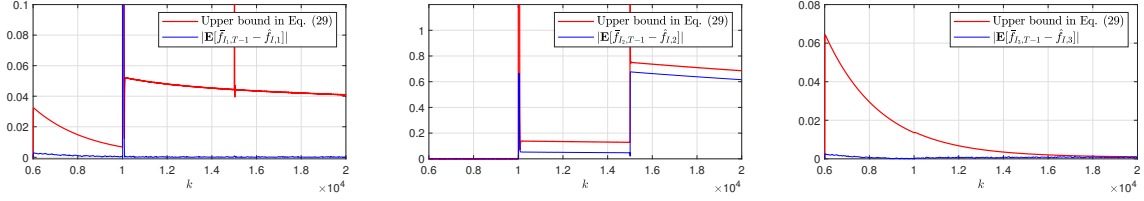
FIGURE 12. Residual $\tilde{\Upsilon}_{1,T}$ for isolation of the incipient power line fault $f_{I,1}$.

FIGURE 13. Performance bounds derived by Theorem 4.3.

noise. A key contribution is the analysis of the coupling effect between power load variations and faulty line currents, an aspect previously underexplored in DC microgrids. To address this challenge, we introduce a novel differentiate-before-estimate strategy that enhances fault detection accuracy. Future work will extend this approach to more generalized load conditions, including nonlinear ZIP (constant impedance, constant current, and constant power) loads, as well as plug-and-play operation scenarios.

APPENDIX A.

Proof of Proposition 4.1. In the first part of the proof, we show that the effect of a step load change on $\tilde{\Upsilon}_{i,T}$ will vanish after T steps. Suppose that P_i becomes $\bar{P}_i = P_i + \Delta P_i$ at some time instant $k_0 \in [k - T + 1, k - 1]$. Then, $\mathbf{v}_{i,T-1}$ can be divided into two parts accordingly, i.e.,

$$\mathbf{v}_{i,T-1}(k-1) = \begin{bmatrix} \mathbf{v}_{i,k_0-(k-T+1)}(k_0-1) \\ \mathbf{v}_{i,k-k_0}(k-1) \end{bmatrix}.$$

The parity space equation (20) in the presence of the step load change can be written as

$$\Upsilon_{i,T} = \Psi_{i,T} P_i + \begin{bmatrix} \mathbf{0} \\ \mathbf{v}_{i,k-k_0} \end{bmatrix} \Delta P_i + \Omega_{i,T}.$$

Substituting $\Upsilon_{i,T}$ into (21) leads to

$$\hat{P}_i = P_i + \Phi_{i,T} \begin{bmatrix} \mathbf{0} \\ \mathbf{v}_{i,k-k_0} \end{bmatrix} \Delta P_i + \Phi_{i,T} \Omega_{i,T},$$

where $\Phi_{i,T}\Psi_{i,T} = \mathbf{I}$ is used here. Then, based on (22), the expectation of the estimation error $\mathbf{E}[\tilde{\Upsilon}_{i,T}]$ becomes

$$\mathbf{E}[\tilde{\Upsilon}_{i,T}] = (\mathbf{I}_{n_Y} - \Psi_{i,T}\Phi_{i,T}) \begin{bmatrix} \mathbf{0} \\ \mathbf{v}_{i,k-k_0} \end{bmatrix} \Delta P_i,$$

which is no longer zero because of ΔP_i . Thus, entries of $\tilde{\Upsilon}_{i,T}$ can exceed the threshold interval when $k \in [k_0 + 1, k_0 + T - 2]$.

For $k \geq k_0 + T - 1$, namely, T steps after the power load change, the estimation result in (21) becomes unbiased again because $\Upsilon_{i,T} = \Psi_{i,T}\bar{P}_i + \Omega_{i,T}$. Thus, entries of $\tilde{\Upsilon}_{i,T}$ will lie within the threshold interval with the probability greater than $1 - 1/\alpha^2$ according to Chebyshev's inequality. This completes the first part of the proof.

In the second part of the proof, to show the effects of line faults on $\tilde{\Upsilon}_{i,T}$, let us rewrite the expression of $\Upsilon_{i,T}$ in (20) with line faults, which becomes

$$\Upsilon_{i,T} = \Psi_{i,T}P_i + \mathcal{O}_{i,T}^\perp \mathcal{Z}_{i_1,T} \mathbf{f}_{I_i,T-1} + \Omega_{i,T}.$$

The residual $\tilde{\Upsilon}_{i,T}$ and its expected value are then given by

$$\begin{aligned} \tilde{\Upsilon}_{i,T} &= \Upsilon_{i,T} - \Psi_{i,T}\Phi_{i,T}\Upsilon_{i,T} \\ &= (\mathbf{I}_{n_Y} - \Psi_{i,T}\Phi_{i,T})(\mathcal{O}_{i,T}^\perp \mathcal{Z}_{i_1,T} \mathbf{f}_{I_i,T-1} + \Omega_{i,T}), \\ \mathbf{E}[\tilde{\Upsilon}_{i,T}] &= (\mathbf{I}_{n_Y} - \Psi_{i,T}\Phi_{i,T})\mathcal{O}_{i,T}^\perp \mathcal{Z}_{i_1,T} \mathbf{f}_{I_i,T-1} \neq \mathbf{0}. \end{aligned}$$

Different from the effects of step load changes ΔP_i that vanish after T steps, the line faults can be distinguished from ΔP_i if there exists $\kappa \in \{1, \dots, n_Y\}$ such that $\tilde{\Upsilon}_{i,T}^{[\kappa]}(k) \notin [-\varepsilon_i^{[\kappa]}(k), \varepsilon_i^{[\kappa]}(k)]$ for at least T consecutive steps. This completes the proof. \square

APPENDIX B.

To prove Theorem 4.3, we introduce the following lemma.

Lemma B.1 (Eigenvalue bounds of a matrix). *The matrix*

$$\mathcal{M}_{i,T} = \begin{bmatrix} \mathcal{M}_{i,T}^{[11]} & \mathcal{M}_{i,T}^{[12]} \\ \mathcal{M}_{i,T}^{[21]} & \mathcal{M}_{i,T}^{[22]} \end{bmatrix} = \begin{bmatrix} \Psi_{i,T}^\top \Psi_{i,T} & \Psi_{i,T}^\top \bar{\mathcal{Z}}_{i,T} \\ \bar{\mathcal{Z}}_{i,T}^\top \Psi_{i,T} & \bar{\mathcal{Z}}_{i,T}^\top \bar{\mathcal{Z}}_{i,T} \end{bmatrix}$$

is bounded by $\underline{\lambda}_{\mathcal{M}_{i,T}} \mathbf{I}_2 \preceq \mathcal{M}_{i,T} \preceq \bar{\lambda}_{\mathcal{M}_{i,T}} \mathbf{I}_2$.

Proof. Since $\mathcal{M}_{i,T}$ is a 2×2 matrix, the larger eigenvalue of $\mathcal{M}_{i,T}$ satisfies

$$\frac{\mathcal{M}_{i,T}^{[11]} + \mathcal{M}_{i,T}^{[22]} + \sqrt{\Xi_{i,T}}}{2} \leq \mathcal{M}_{i,T}^{[11]} + \mathcal{M}_{i,T}^{[22]} = \Psi_{i,T}^\top \Psi_{i,T} + \bar{\mathcal{Z}}_{i,T}^\top \bar{\mathcal{Z}}_{i,T} = \bar{\lambda}_{\mathcal{M}_{i,T}},$$

where $\Xi_{i,T} = \left(\mathcal{M}_{i,T}^{[11]} + \mathcal{M}_{i,T}^{[22]} \right)^2 - 4 \left(\mathcal{M}_{i,T}^{[11]} \mathcal{M}_{i,T}^{[22]} - \mathcal{M}_{i,T}^{[12]^2} \right)$. The above inequality holds because of the Cauchy-Schwarz inequality, i.e.,

$$\mathcal{M}_{i,T}^{[11]} \mathcal{M}_{i,T}^{[22]} - \mathcal{M}_{i,T}^{[12]^2} = \Psi_{i,T}^\top \Psi_{i,T} \bar{\mathcal{Z}}_{i,T}^\top \bar{\mathcal{Z}}_{i,T} - \Psi_{i,T}^\top \bar{\mathcal{Z}}_{i,T} \bar{\mathcal{Z}}_{i,T}^\top \Psi_{i,T} \geq 0.$$

For the smaller eigenvalue of $\mathcal{M}_{i,T}$, it holds that

$$\frac{\mathcal{M}_{i,T}^{[11]} + \mathcal{M}_{i,T}^{[22]} - \sqrt{\Xi_{i,T}}}{2} = \frac{2 \left(\mathcal{M}_{i,T}^{[11]} \mathcal{M}_{i,T}^{[22]} - \mathcal{M}_{i,T}^{[12]^2} \right)}{\mathcal{M}_{i,T}^{[11]} + \mathcal{M}_{i,T}^{[22]} + \sqrt{\Xi_{i,T}}} \geq \frac{\mathcal{M}_{i,T}^{[11]} \mathcal{M}_{i,T}^{[22]} - \mathcal{M}_{i,T}^{[12]^2}}{\mathcal{M}_{i,T}^{[11]} + \mathcal{M}_{i,T}^{[22]}} = \lambda_{\mathcal{M}_{i,T}}.$$

This is because $\Xi_{i,T} \leq \left(\mathcal{M}_{i,T}^{[11]} + \mathcal{M}_{i,T}^{[22]} \right)^2$. This completes the proof. \square

Proof of Theorem 4.3. Based on the analytical solution given in (28), the estimation error of Θ_i can be written as

$$\Theta_i - \hat{\Theta}_i = \Theta_i - \mathcal{K}_{i,T}^{-1} \left(\Gamma_{i,T}^\top \Sigma_{\Omega_{i,T}}^{-1} \Upsilon_{i,T} + \eta \nu_1^\top \nu_1 \hat{\Theta}_{i-} + \eta \nu_1^\top \nu_1 \Theta_i - \eta \nu_1^\top \nu_1 \Theta_i \right).$$

Substituting $\Upsilon_{i,T}$ in (26) into the above equation leads to

$$\begin{aligned} \Theta_i - \hat{\Theta}_i &= \Theta_i - \mathcal{K}_{i,T}^{-1} \left(\Gamma_{i,T}^\top \Sigma_{\Omega_{i,T}}^{-1} \Gamma_{i,T} + \eta \nu_1^\top \nu_1 \right) \Theta_i \\ &\quad - \mathcal{K}_{i,T}^{-1} \Gamma_{i,T}^\top \Sigma_{\Omega_{i,T}}^{-1} \left(\mathcal{O}_{i,T}^\perp \mathcal{Z}_{i1,T} (\Delta \mathbf{f}_{I,T-1} + \Delta \mathbf{P}_i) + \Omega_{i,T} \right) + \mathcal{K}_{i,T}^{-1} \eta \nu_1^\top \nu_1 (\Theta_i - \hat{\Theta}_{i-}) \\ &= - \mathcal{K}_{i,T}^{-1} \Gamma_{i,T}^\top \Sigma_{\Omega_{i,T}}^{-1} \left(\mathcal{O}_{i,T}^\perp \mathcal{Z}_{i1,T} (\Delta \mathbf{f}_{I,T-1} + \Delta \mathbf{P}_i) + \Omega_{i,T} \right) + \mathcal{K}_{i,T}^{-1} \eta \nu_1^\top \nu_1 (\Theta_i - \hat{\Theta}_{i-}), \end{aligned}$$

Recall that $\mathcal{K}_{i,T} = \Gamma_{i,T}^\top \Sigma_{\Omega_{i,T}}^{-1} \Gamma_{i,T} + \eta \nu_1^\top \nu_1$. Since $\bar{f}_{I,T-1} - \hat{f}_{I,i} = [0 \ 1](\Theta_i - \hat{\Theta}_i)$, the absolute value of $\mathbf{E}[\bar{f}_{I,T-1} - \hat{f}_{I,i}]$ is bounded by

$$\begin{aligned} \left| \mathbf{E} [\bar{f}_{I,T-1} - \hat{f}_{I,i}] \right| &\leq \left\| \mathcal{K}_{i,T}^{-1} \right\|_2 \left\| \Gamma_{i,T}^\top \right\|_2 \left\| \Sigma_{\Omega_{i,T}}^{-1} \right\|_2 \left\| \mathcal{O}_{i,T}^\perp \mathcal{Z}_{i1,T} \right\|_2 \times \\ &\quad \left(\|\Delta \mathbf{f}_{I,T-1}\|_2 + \|\Delta \mathbf{P}_i\|_2 \right) + |[0 \ 1] \mathcal{K}_{i,T}^{-1} \eta \nu_1^\top \nu_1 (\Theta_i - \hat{\Theta}_{i-})|. \end{aligned} \quad (31)$$

According to Lemma B.1, matrix $\mathcal{K}_{i,T}$ is lower bounded by

$$\begin{aligned} \mathcal{K}_{i,T} &= \Gamma_{i,T}^\top \Sigma_{\Omega_{i,T}}^{-1} \Gamma_{i,T} + \eta \nu_1^\top \nu_1 \\ &\succeq \frac{1}{\bar{\lambda}_{\Sigma_{\Omega_{i,T}}}} \begin{bmatrix} \Psi_{i,T}^\top \Psi_{i,T} & \Psi_{i,T}^\top \bar{\mathcal{Z}}_{i,T} \\ \bar{\mathcal{Z}}_{i,T}^\top \Psi_{i,T} & \bar{\mathcal{Z}}_{i,T}^\top \bar{\mathcal{Z}}_{i,T} \end{bmatrix} + \eta \nu_1^\top \nu_1 \\ &\succeq \frac{\lambda_{\mathcal{M}_{i,T}}}{\bar{\lambda}_{\Sigma_{\Omega_{i,T}}}} I + \eta \nu_1^\top \nu_1. \end{aligned}$$

Moreover, since the 2-norm $\|\mathcal{K}_{i,T}^{-1}\|_2 = \bar{\lambda}_{\mathcal{K}_{i,T}}^{-1} = 1/\lambda_{\mathcal{K}_{i,T}}$, $\|\mathcal{K}_{i,T}^{-1}\|_2$ is upper bounded by

$$\left\| \mathcal{K}_{i,T}^{-1} \right\|_2 \leq \frac{\bar{\lambda}_{\Sigma_{\Omega_{i,T}}}}{\lambda_{\mathcal{M}_{i,T}} + \eta \bar{\lambda}_{\Sigma_{\Omega_{i,T}}}}. \quad (32)$$

For $\left\| \Gamma_{i,T}^\top \right\|_2$, according to Lemma B.1, we have

$$\left\| \Gamma_{i,T}^\top \right\|_2 = \sqrt{\left\| \Gamma_{i,T}^\top \Gamma_{i,T} \right\|_2} = \sqrt{\lambda_{\mathcal{M}_{i,T}}}. \quad (33)$$

Together with (32) and (33), the first component on the right-hand side of inequality (31) is upper bounded by

$$\left\| \mathcal{K}_{i,T}^{-1} \right\|_2 \left\| \Gamma_{i,T}^\top \right\|_2 \left\| \Sigma_{\Omega_{i,T}}^{-1} \right\|_2 \left\| \mathcal{O}_{i,T}^\perp \mathcal{Z}_{i1,T} \right\|_2 \leq \frac{\bar{\lambda}_{\Sigma_{\Omega_{i,T}}}}{\lambda_{\mathcal{M}_{i,T}} + \eta \bar{\lambda}_{\Sigma_{\Omega_{i,T}}}} \frac{\sqrt{\lambda_{\mathcal{M}_{i,T}}}}{\lambda_{\Sigma_{\Omega_{i,T}}}} \bar{\sigma}(\mathcal{O}_{i,T}^\perp \mathcal{Z}_{i1,T}). \quad (34)$$

For the second term on the right-hand side of inequality (31), it holds that

$$[0 \ 1]\mathcal{K}_{i,T}^{-1}\eta\nu_1^\top\nu_1(\Theta_i - \hat{\Theta}_{i-}) = \frac{-\bar{\mathcal{Z}}_{i,T}^\top\Sigma_{\Omega_{i,T}}^{-1}\Psi_{i,T}\eta(P_i - \hat{P}_{i-})}{\det(\mathcal{K}_{i,T})},$$

where the inverse term $\mathcal{K}_{i,T}^{-1}$ is computed in the above equation. The determinant of $\mathcal{K}_{i,T}$ satisfies the following inequality:

$$\begin{aligned}\det(\mathcal{K}_{i,T}) &= \left(\bar{\mathcal{Z}}_{i,T}^\top\Sigma_{\Omega_{i,T}}^{-1}\bar{\mathcal{Z}}_{i,T}\right) \left(\Psi_{i,T}^\top\Sigma_{\Omega_{i,T}}^{-1}\Psi_{i,T} + \eta\right) - \left(\Psi_{i,T}^\top\Sigma_{\Omega_{i,T}}^{-1}\bar{\mathcal{Z}}_{i,T}\right) \left(\bar{\mathcal{Z}}_{i,T}^\top\Sigma_{\Omega_{i,T}}^{-1}\Psi_{i,T}\right) \\ &\geq \bar{\mathcal{Z}}_{i,T}^\top\Sigma_{\Omega_{i,T}}^{-1}\bar{\mathcal{Z}}_{i,T}\eta.\end{aligned}$$

As a result, we have

$$\left|[0 \ 1]\mathcal{K}_{i,T}^{-1}\eta\nu_1^\top\nu_1(\Theta_i - \hat{\Theta}_{i-})\right| \leq \frac{\bar{\mathcal{Z}}_{i,T}^\top\Sigma_{\Omega_{i,T}}^{-1}\Psi_{i,T}|P_i - \hat{P}_{i-}|}{\bar{\mathcal{Z}}_{i,T}^\top\Sigma_{\Omega_{i,T}}^{-1}\bar{\mathcal{Z}}_{i,T}} \leq \frac{\bar{\lambda}_{\Sigma_{\Omega_{i,T}}}\bar{\mathcal{Z}}_{i,T}^\top\Psi_{i,T}|P_i - \hat{P}_{i-}|}{\underline{\lambda}_{\Sigma_{\Omega_{i,T}}}\bar{\mathcal{Z}}_{i,T}^\top\bar{\mathcal{Z}}_{i,T}}. \quad (35)$$

Together with inequalities (34) and (35), the estimation error bound (29) is derived. This completes the proof. \square

REFERENCES

- [1] A. M. Mohamad, Y. A.-R. I. Mohamed, Investigation and assessment of stabilization solutions for DC microgrid with dynamic loads, *IEEE Transactions on Smart Grid* 10 (5) (2019) 5735–5747.
- [2] M. Salehi, S. A. Taher, I. Sadeghkhan, M. Shahidehpour, A poverty severity index-based protection strategy for ring-bus low-voltage DC microgrids, *IEEE Transactions on Smart Grid* 10 (6) (2019) 6860–6869.
- [3] A. A. Emhemed, K. Fong, S. Fletcher, G. M. Burt, Validation of fast and selective protection scheme for an LVDC distribution network, *IEEE Transactions on Power Delivery* 32 (3) (2016) 1432–1440.
- [4] S. Dhar, R. K. Patnaik, P. Dash, Fault detection and location of photovoltaic based DC microgrid using differential protection strategy, *IEEE Transactions on Smart Grid* 9 (5) (2017) 4303–4312.
- [5] A. Meghwhani, S. Srivastava, S. Chakrabarti, A non-unit protection scheme for DC microgrid based on local measurements, *IEEE Transactions on Power Delivery* 32 (1) (2016) 172–181.
- [6] K. A. Saleh, A. Hooshyar, E. F. El-Saadany, Ultra-high-speed traveling-wave-based protection scheme for medium-voltage DC microgrids, *IEEE Transactions on Smart Grid* 10 (2) (2017) 1440–1451.
- [7] M. H. R. A. Syafi'i, E. Prasetyono, M. K. Khafidli, D. O. Anggriawan, A. Tjahjono, Real time series DC arc fault detection based on fast Fourier transform, in: *2018 International Electronics Symposium on Engineering Technology and Applications (IES-ETA)*, IEEE, 2018, pp. 25–30.
- [8] X. Yao, L. Herrera, S. Ji, K. Zou, J. Wang, Characteristic study and time-domain discrete-wavelet-transform based hybrid detection of series DC arc faults, *IEEE Transactions on Power Electronics* 29 (6) (2013) 3103–3115.
- [9] P. Pan, R. K. Mandal, Learning approach based DC arc fault location classification in DC microgrids, *Electric Power Systems Research* 208 (2022) 107874.
- [10] T. Wang, C. Zhang, Z. Hao, A. Monti, F. Ponci, Data-driven fault detection and isolation in DC microgrids without prior fault data: A transfer learning approach, *Applied Energy* 336 (2023) 120708.
- [11] Z. Gao, C. Cecati, S. X. Ding, A survey of fault diagnosis and fault-tolerant techniques—part I: Fault diagnosis with model-based and signal-based approaches, *IEEE Transactions on Industrial Electronics* 62 (6) (2015) 3757–3767.
- [12] M. Nyberg, E. Frisk, Residual generation for fault diagnosis of systems described by linear differential-algebraic equations, *IEEE Transactions on Automatic Control* 51 (12) (2006) 1995–2000.
- [13] X. Yao, V. Le, I. Lee, Unknown input observer-based series DC arc fault detection in DC microgrids, *IEEE Transactions on Power Electronics* 37 (4) (2021) 4708–4718.
- [14] T. Wang, L. Liang, S. K. Gurumurthy, F. Ponci, A. Monti, Z. Yang, R. W. De Doncker, Model-based fault detection and isolation in DC microgrids using optimal observers, *IEEE Journal of Emerging and Selected Topics in Power Electronics* 9 (5) (2020) 5613–5630.
- [15] T. Wang, L. Liang, Z. Hao, A. Monti, F. Ponci, LPV model-based fault detection and isolation in DC microgrids through signature recognition, *IEEE Transactions on Smart Grid* 14 (4) (2022) 2558–2571.

- [16] A. Vafamand, B. Moshiri, N. Vafamand, Fusing unscented Kalman filter to detect and isolate sensor faults in DC microgrids with CPLs, *IEEE Transactions on Instrumentation and Measurement* 71 (2021) 1–8.
- [17] P. Mohajerin Esfahani, J. Lygeros, A tractable fault detection and isolation approach for nonlinear systems with probabilistic performance, *IEEE Transactions on Automatic Control* 61 (3) (2015) 633–647.
- [18] K. Pan, P. Palensky, P. Mohajerin Esfahani, Dynamic anomaly detection with high-fidelity simulators: A convex optimization approach, *IEEE Transactions on Smart Grid* 13 (2) (2021) 1500–1515.
- [19] J. Dong, Y. Liao, H. Xie, J. Cremer, P. Esfahani Mohajerin, Real-time ground fault detection for inverter-based microgrid systems, *IEEE Transactions on Control Systems Technology* (2024).
- [20] S. Asadi, N. Vafamand, M. Moallem, T. Dragičević, Fault reconstruction of islanded nonlinear DC microgrids: An LPV-based sliding mode observer approach, *IEEE Journal of Emerging and Selected Topics in Power Electronics* 9 (4) (2020) 4606–4614.
- [21] K. Wan, J. Zhao, Y. Chen, M. Yu, A decentralized resilient control scheme for DC microgrids against faults on sensor and actuator, *IEEE Transactions on Circuits and Systems I: Regular Papers* 71 (2) (2023) 816–827.
- [22] A. Cecilia, S. Sahoo, T. Dragičević, R. Costa-Castelló, F. Blaabjerg, Detection and mitigation of false data in cooperative DC microgrids with unknown constant power loads, *IEEE Transactions on Power Electronics* 36 (8) (2021) 9565–9577.
- [23] P. Nahata, R. Soloperto, M. Tucci, A. Martinelli, G. Ferrari-Trecate, A passivity-based approach to voltage stabilization in dc microgrids with ZIP loads, *Automatica* 113 (2020) 108770.
- [24] M. Tucci, S. Rivero, G. Ferrari-Trecate, Line-independent plug-and-play controllers for voltage stabilization in DC microgrids, *IEEE Transactions on Control Systems Technology* 26 (3) (2017) 1115–1123.
- [25] M. S. Sadabadi, Q. Shafiee, Scalable robust voltage control of DC microgrids with uncertain constant power loads, *IEEE Transactions on Power Systems* 35 (1) (2019) 508–515.
- [26] M. Tucci, S. Rivero, J. C. Vasquez, J. M. Guerrero, G. Ferrari-Trecate, A decentralized scalable approach to voltage control of dc islanded microgrids, *IEEE Transactions on Control Systems Technology* 24 (6) (2016) 1965–1979.
- [27] F. Boem, S. Rivero, G. Ferrari-Trecate, T. Parisini, Plug-and-play fault detection and isolation for large-scale nonlinear systems with stochastic uncertainties, *IEEE Transactions on Automatic Control* 64 (1) (2018) 4–19.
- [28] C. P. Robert, G. Casella, G. Casella, Monte Carlo statistical methods, Vol. 2, Springer, 1999.
- [29] S. X. Ding, Model-based Fault Diagnosis Techniques: Design Schemes, Algorithms, and Tools, Springer Science & Business Media, 2008.
- [30] C. Van der Ploeg, M. Alirezaei, N. Van De Wouw, P. Mohajerin Esfahani, Multiple faults estimation in dynamical systems: Tractable design and performance bounds, *IEEE Transactions on Automatic Control* 67 (9) (2022) 4916–4923.
- [31] A. Kwasinski, C. N. Onwuchekwa, Dynamic behavior and stabilization of DC microgrids with instantaneous constant-power loads, *IEEE Transactions on Power Electronics* 26 (3) (2010) 822–834.
- [32] C. Scherer, P. Gahinet, M. Chilali, Multiobjective output-feedback control via LMI optimization, *IEEE Transactions on automatic control* 42 (7) (2002) 896–911.
- [33] J. Dong, A. S. Kolarijani, P. Mohajerin Esfahani, Multimode diagnosis for switched affine systems with noisy measurement, *Automatica* 151 (2023) 110898.
- [34] D. G. Luenberger, Optimization by vector space methods, John Wiley & Sons, 1997.
- [35] M. S. Sadabadi, A resilient-by-design distributed control framework for cyber-physical DC microgrids, *IEEE Transactions on Control Systems Technology* (2023).
- [36] J. Lofberg, YALMIP: A toolbox for modeling and optimization in MATLAB, in: 2004 IEEE International Conference on Robotics and Automation, IEEE, 2004, pp. 284–289.